AN ABSTRACT OF THE THESIS OF

ROBERT BLICKENSDERFER   for the   DOCTOR OF PHILOSOPHY

        (Name)   (Degree)

in   METALLURGICAL ENGINEERING (MATERIALS SCIENCE)   presented on May 15, 1972

                                                                   (Date)

Title: CREEP OF TUNGSTEN DISPERSION STRENGTHENED BY ZrO_2

Redacted for Privacy

Abstract approved: _____

                     Dr. John A. McComb

Tungsten alloys containing approximately 0.75 and 2.3 vol pct ZrO_2 were prepared by powder metallurgical methods from blends of commercial tungsten powder and ZrW_2 powder. A heat treatment of the extruded rods at 1800°C was found to produce a stable structure with a dispersion of ZrO_2 particles in the tungsten matrix. The mean particle size was about 0.2 µm, the mean particle spacing about 2 µm, and the mean tungsten grain size about 7 µm. There was essentially no difference in microstructure between the two alloys except the 2.3 vol pct ZrO_2 alloy contained more of the coarse ZrO_2 stringers.

The tensile strength of the alloys ranged from 45 ksi at 1500°C to 25 ksi at 2000°C. Stress rupture lives were determined at 1375°C and 1740°C over a stress range of 10 to 60 ksi.

Creep measurements were made over the temperature range of 1465° to 1924°C and over a stress range of 3.5 to 20 ksi. The activation energy for creep was found to be a constant 104,200 ± 3,200 cal per g mole °K over the entire range of stress and over the temperature range of 1500° to 1800°C. The activation volume was calculated as 1.3×10^{-21} cm^3. The creep rate was found to vary linearly with stress in the low stress region ($\sigma < 12$ ksi), and to vary as stress to the power of 4.6 in the high stress region ($\sigma > 14$ ksi).

The creep behavior of these tungsten alloys fits the functional relationships of stress and temperature given by the Ansell-Weertman model for dispersion strengthened alloys at both low and high stresses. However, the values of creep rate calculated from the model are about 10^3 times greater than the experimental values. The Nabarro-Herring creep model fits the creep behavior of the tungsten alloys at low stresses both with respect to the functional dependence and the values of creep rate.

A modification of the Ansell-Weertman model in the high stress region is made in which the area swept out by a dislocation corresponding to a unit of climb is taken as of the order of λ^2 where λ is the planar interparticle spacing. The density of active Frank-Read sources is taken as 10^9 per cm^3. This modified Ansell-Weertman model is shown to satisfy the stress and temperature relationships for creep of the tungsten alloys and to give values of creep rate which agree very well with experimental results. The modified model is also shown to provide the correction of 10^4 needed to satisfy earlier experimental results on dispersion strengthened aluminum.

Creep of Tungsten Dispersion
Strengthened by ZrO_2

by

Robert Blickensderfer

A THESIS

submitted to

Oregon State University

in partial fulfillment of
the requirements for the
degree of

Doctor of Philosophy

June 1972

APPROVED:

Redacted for Privacy

Professor of Metallurgical Engineering
in charge of major

Redacted for Privacy

Head of Department of Metallurgical Engineering

Redacted for Privacy

Dean of Graduate School

Date thesis is presented May 15, 1972

Typed by Bernice Wirowek for Robert Blickensderfer

Symbol	Description
A	Constant
B	Constant
C	Constant
C_O	Vacancy concentration
D	Diffusion coefficient
D_O	Diffusion constant
F-R	Frank-Read source
L	Maximum radius of a dislocation loop
M	Density of active dislocation sources
N	Number of piled up dislocations
N_s	Number of particles in a plane
Q	Activation energy
R	Gas constant
S	Area
T	Temperature
T_{mp}	Melting point temperature
V^*	Activation volume
a_O	Lattice constant
b	Length of a Burger's vector
b_c	Corrected value of intercept
d	Distance climbed by a dislocation

Symbol	Description
h	Mean particle size of dispersoid
k	Boltzman's constant
Δl	Mean intercept length in a plane
ℓ	Mean dimension of grains
m	Slope of a linear equation
n	Power of the stress dependency
q	Flow rate of vacancies
r	Rate of creation of dislocations
v	Velocity of climb, (speed)
α	Constant
$\dot{\varepsilon}$	Creep rate
λ	Mean spacing of dispersoid particles
Λ	Perpendicular distance between dislocation loops
ρ	Radius of curvature
σ	Stress
μ	Shear modulus
Ω	Volume of a vacancy

TABLE OF CONTENTS

CREEP OF TUNGSTEN DISPERSION STRENGTHENED BY ZrO_2

I. INTRODUCTION

Tungsten Alloy Development

For material applications at high temperatures and high stresses, the creep behavior and stress rupture life are two of the most important mechanical properties. Tungsten, with the highest melting point (3410°C) of all metals, has the greatest potential for creep resistance because of the relationships between strength, creep activation energy, and melting temperature shown by Dorn [20]. Early studies on $W-ThO_2$ alloys, from 1916 to 1924 by Jefferies [37], showed that ThO_2 particles effectively restrained tungsten grain growth until heated to about 2500°C.

After World War II much effort was devoted to develop improved tungsten-base materials. Most of the effort, until the past six to eight years was expended on improving the high temperature strength with solutes [19,71]. Additional methods for strengthening tungsten included fibered composites by Quatinetz et al [58], carbide precipitation strengthening by Raffo and Klopp [60], and dispersion strengthening by Sell [66-70], Morcom [48], and Kane [38].

The tungsten alloy used in the present work was a ZrO_2 dispersion strengthened material known as ZOW alloy. It was developed by Mark I. Copeland at the Albany Metallurgy Research Center, Bureau of Mines, and is described fully in reference [11]. In the extruded condition, the ZOW

alloy possessed tensile and stress-rupture properties superior to any

commercial tungsten alloys. The tensile strength of the strongest ZOW

alloy at 1650°C in the extruded condition was 70,000 psi compared to

30,000 psi for W-2ThO$_2$ in the swaged condition [19]. The stress-rupture

life of the ZOW alloy at 10,000 psi and 1650°C was at least 100 hours

compared to about 30 hours for commercial W-3.7 vol pct ThO$_2$ under the

same conditions [11]. The nominal composition of the original ZOW alloy

was about 0.4 wt pct Zr and 0.07 wt pct oxygen. The nominal ZrO$_2$ content

was 1 vol pct.

Creep Theory of Dispersion Strengthened Alloys

The theories of creep, in general, have been summarized and reviewed

a number of times [20,24,28,46,49,54,64,82]. With the advent of the dis-

persion strengthened SAP alloys (sintered aluminum powder) and TD nickel

(thoria-dispersed nickel) and their remarkable creep resistance at high

homologous temperatures, interest in the creep theory of dispersion

strengthened structures was aroused.

An early model provided a mechanism for strengthening of two phase

structures based on the interference of dislocation motion by second

phase particles. The model, known as the Orowan bowing model, introduced

by Orowan [56] in 1948, has survived to the present time. The model

pictures the second phase particles as blocking the dislocations. As the

stress is increased, the dislocations bow between the particles, event-

ually breaking away and leaving a closed dislocation loop around the

particle.

Ansell and Lenel [4] proposed a model to account for the yielding
behavior of dispersion-strengthened alloys. The criteria for yielding
used in the model, was that appreciable yielding occurred when the
shear stress due to piled-up groups of dislocations was sufficient to
fracture or plastically deform the dispersed second-phase particles.
The model did not consider deformation by creep which might be possible
at lower stresses.

Ansell and Weertman [6] developed a model for creep of dispersion
strengthened alloys based on dislocation climb. The theory was based
on earlier work of Weertman [80-82] for single-phase alloys which was
due essentially to the theory of Mott [49]. According to the Ansell-
Weertman model, dislocation loops are created at sources under the
action of an applied stress. The loops expand to some maximum radius
at which time they are annihilated by climbing to dislocations of oppo-
site sign on neighboring slip planes. The rate controlling process
for steady state creep was assumed to be the climb of dislocations over
the dispersed-phase particles. Ansell and Weertman arrived at ex-
pressions which permitted the calculation of steady state creep rate
based on fundamental quantities. They showed that $\dot{\varepsilon}$, the steady state
creep rate, should vary linearly with stress at low stresses, and
should vary as the fourth power of stress, σ^4, at high stresses. In a
review of the literature concerning creep in single phase alloys,
Weertman [81] showed that most creep data fit a power dependence of the
form $\dot{\varepsilon} \propto \sigma^n$. The value of n ranged from 2 to 5.5 with values near 4
being the most common. These theories employed an activation energy

for creep equal to that for self-diffusion. Confirmation of the Ansell-Weertman model for dispersion strengthened alloys was only partially successful. The σ^4 stress dependency on $\dot{\epsilon}$ was found for a SAP alloy but the linear dependency was not found and the absolute values of creep rate calculated from the theory were 10^4 times higher than the experimental values.

Mott [49] proposed that the glide movement of dislocations is the rate controlling process for creep while their disappearance by climb is fast enough to prevent work hardening. At low stresses, the creep rate should be linear with both stress and the diffusion coefficient. The movement, with dislocations impeded by an atmosphere of solute atoms, should show viscous behavior. Above a certain stress the dislocation breaks away from the atmosphere and a sudden increase in creep rate should occur. At high stresses Mott proposed that the rate controlling process during steady-state creep was the production of vacancies by moving jogs in screw dislocations. He then developed an expression for the activation energy for creep which contained terms for the formation and migration energy of vacancies minus a stress term. A marked dependency of the activation energy on the stress should result if the model is applicable.

Purpose of the Study

The purpose of the study was several-fold; some of the desired results were of an engineering nature, others of a theoretical nature.

The major objectives were:

1. To develop a heat treatment for the ZOW alloy
which would result in a microstructure which was
stable at temperatures up to 1700°C. Hopefully, the
heat treatment would further improve the mechanical
properties over those in the as-extruded condition.

2. To synthesize a ZOW alloy of higher zirconium
and oxygen content than the nominal 1 vol pct ZrO_2,
and to determine the effect of the greater volume
fraction of ZrO_2 on the elevated temperature properties.

3. To acquire tensile and stress-rupture data on
the alloys at elevated temperature in order to better
characterize their mechanical properties.

4. To find a creep model which would account for
the creep behavior of the dispersion strengthened
ZOW alloys.

II. EXPERIMENTAL PROCEDURE

General

Specimens were prepared by powder metallurgical methods from blends of commercial tungsten powders and a ZrW_2 powder made by the author. The procedure for synthesizing such dispersion strengthened alloys is given in greater detail in reference [11/].

Composition of Alloys

Alloys of two compositions were made in an effort to obtain materials with two different ZrO_2 contents. Based on previous work, both alloys were prepared to have enough Zr to combine with the oxygen present in the tungsten powder plus an additional 0.3 wt pct Zr. One alloy, designated as ZOW Alloy type I, was to contain about 0.4 wt pct Zr because this was within the range of Zr which had provided the greatest tensile strength and stress-rupture life at 1650°C in a previous investigation [11/]. The second alloy, designated as ZOW Alloy type II, was to contain appreciably more ZrO_2 but to contain the same 0.3 wt pct Zr beyond the amount necessary to combine with all of the oxygen present. The two different oxygen contents were obtained by using tungsten powder of two different particle sizes. The mean particle size and oxygen content of the two powders was 5.5 micron, 400 ppm, and 2.5 micron, 1100 ppm, respectively. The synthesizing data are given in Table 1. The calculated nominal composition of Alloy I was W-0.47Zr-0.060 O, and that of Alloy II was W-0.82Zr-0.180 O.

TABLE I. Synthesis of the alloys from powders

Alloy type	Source	Tungsten powder		ZrW$_2$ powder			Calculated nominal composition of alloy		
		Nominal size, micron	Oxygen content, ppm [1]	Nominal size, micron	Zr, wt pct	O, ppm	W, wt pct	Zr, wt pct	O, ppm
I	Sylvania, Lot WA-55-143C	5.5	400	20	17.7	540	99.5	0.47	600
II	Sylvania, Lot WA-37-112C	2.5	1100	20	17.7	540	99.0	0.82	1800

[1] The oxygen content normally increased about 50% during mill-blending.

These oxygen contents correspond to 0.75 and 2.3 vol pct ZrO_2 respectively for ZOW type I and II. For comparison, Rezek and Childs [61] found that 2 vol pct yttria in zirconium gave the lowest creep rate.

Seven batches of Alloy I were synthesized, each consisting of 1000 grams of the 5.5 micron tungsten powder and 24 grams of the ZrW_2 powder. Eight batches of Alloy II were made, each from 1000 grams of the 2.5 micron tungsten powder and 41 grams of ZrW_2 powder. The chemical analysis of the specimens after complete synthesis and testing are given in Table II. The mean analyzed composition of Alloy I was W-0.42Zr-0.052 O, and that of Alloy II was W-0.70Zr-0.129 O. This corresponds to 0.70 and 1.6 vol pct ZrO_2 respectively with 0.27 and 0.32 wt pct respectively of uncombined Zr.

Specimen Preparation

The tungsten and ZrW_2 powders were loaded into a rod mill 4 inches in diameter with a volume of 1200 cc. The mill, which was lined with molybdenum, utilized tungsten rods. After adding 500 cc of water, the mill was run for four hours at 107 rpm. The blended powder was allowed to settle, the liquid was decanted, and the powder was dried for two days at room temperature. After breaking up the powder cake, it was passed through a 200-mesh screen.

The dried, blended powder was loaded into a rubber sock and vibratory compacted to approximately 1-3/4 inches diameter by 3-1/4 inches long. The powder was then isostatically compacted at 30,000 psi into a cylindrical body about 1-1/2 inches in diameter by 3 inches long and a density of 11 grams per cm^3.

Table II. Specimen numbers, type, and analysis after testing

| | Specimens | | Chemical analysis | |
| | Stress-rupture | Tensile | Zr, wt pct | O, ppm |
Creep				
Alloy I – Nominal 0.47 wt pct Zr				
17A			0.43	440
17B				
18A			0.44	464
18B				
	19A		0.42	376
	19B		0.40	395
	20A		0.40	594
	20B		0.41	608
		21	0.42	630
22A			0.42	426
22B				
	23		0.42	710
		33A		
Alloy II – Nominal 0.82 wt pct Zr				
	24		0.69	1287
	25A		0.69	1201
	25B		0.69	1250
		26A	0.69	1260
	26B		0.69	1260
	27A		0.69	1342
27B				
27C				
28A			0.71	1132
28B				
29A			0.72	1068
29B				
		34A		
35B			0.71	1205
		36A		
36C			0.70	1867

The compacts were sintered under vacuum at a temperature of 2,000°C for 16 hours. The furnace, which utilized a tungsten resistance heating element, reached 2,000°C after three hours. The pressure in the furnace ranged from a maximum of about 10^{-3} torr during heat up to about 10^{-5} torr at the end of the heating period. The sintered billet, with a density of about 17 grams per cm^3, was machined to 1.250 inches diameter.

The billet was reheated rapidly under flowing argon by induction heating and held at a temperature of 1800 to 2100°C for five minutes. The hot billet was extruded by a Dynapak forge through a 1/2-inch-diameter die which provided an area reduction of six. The extruded rods ranged from 4.8 to 10.3 inches long which provided material for one to three creep or tensile specimens each.

Slices of the extruded rods were used for heat-treating experiments in order to determine the treatment necessary to produce a stable structure with a ZrO_2 dispersion. The aging treatment which was found, 20 hours at 1800°C under vacuum, was subsequently given to the extruded rods.

Rods were then machined into tensile or creep specimens with a nominal test section of 1/4- or 1/8-inch diameter, respectively, as illustrated in Figures 1 and 2.

Testing Procedures

Tensile Testing

Tensile testing was done under vacuum at a strain rate of 0.02 per minute over a temperature range of 1600 to 2000°C on a modified

Marquardt TM-1 machine. The button-head specimens had a reduced section three inches long and 0.25 inch diameter as indicated in Figure 1. The specimen was self-heated by its resistance to an electric current. The temperature was measured by a two-color pyrometer. At midpoint of the specimen, the temperature was held at test temperature $\pm$ 35°C.

Creep and Stress-rupture Testing

The creep and stress-rupture tests were carried out in a Brew vacuum furnace mounted on a Satec test bed. The furnace utilized a tungsten mesh resistance element powered by a silicon controlled rectifier system. The loading was done by a dead weight system, external to the vacuum chamber on a 5 to 1 lever. The vacuum was normally less than 2 x 10^{-6} torr. The button head specimens had a reduced section 1-1/4 inches long and 0.125 inches diameter as shown in Figure 2.

Temperature measurements were made with a calibrated optical pyrometer and a calibrated thermocouple of W5Re-W26Re. The pyrometer readings were corrected for absorption by the window glass; a cold junction of 0°C was used for the thermocouple. In the early part of the test program, during stress-rupture testing, the heating power was controlled by a transducer power unit; however, the temperature was found to drift several degrees C over a period of one or two days. The better control required for creep tests was obtained with thermocouple control.

Temperature measurements were made in black body holes of .015 inch diameter in a 1/8-inch-diameter molybdenum rod. The rod was located alongside the 1/8-inch-diameter test section of the creep specimen, as shown in Figure 3. A thermocouple, made from wires of 0.005
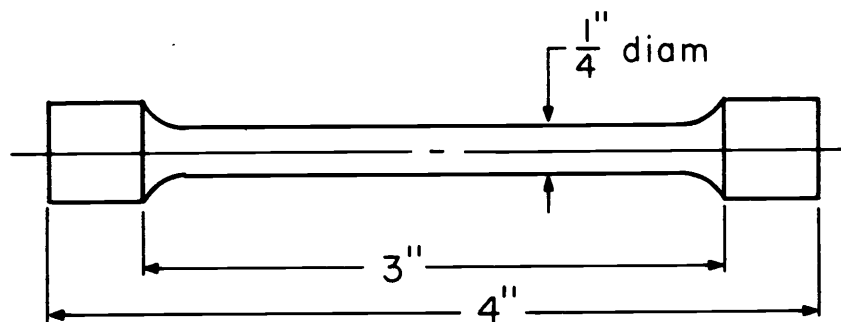
FIGURE 1.-Button Head Tensile Specimen.
Nominal 1/4-inch round, for high temp-
erature self resistance heating.
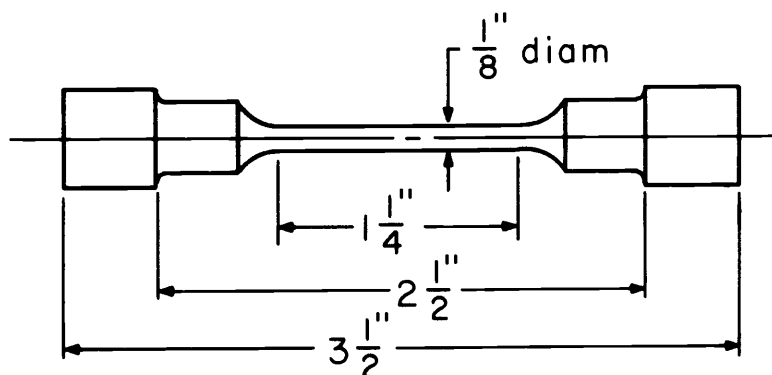
FIGURE 2.-Button Head Creep Specimen
Nominal 1/8 inch Round.

72-129
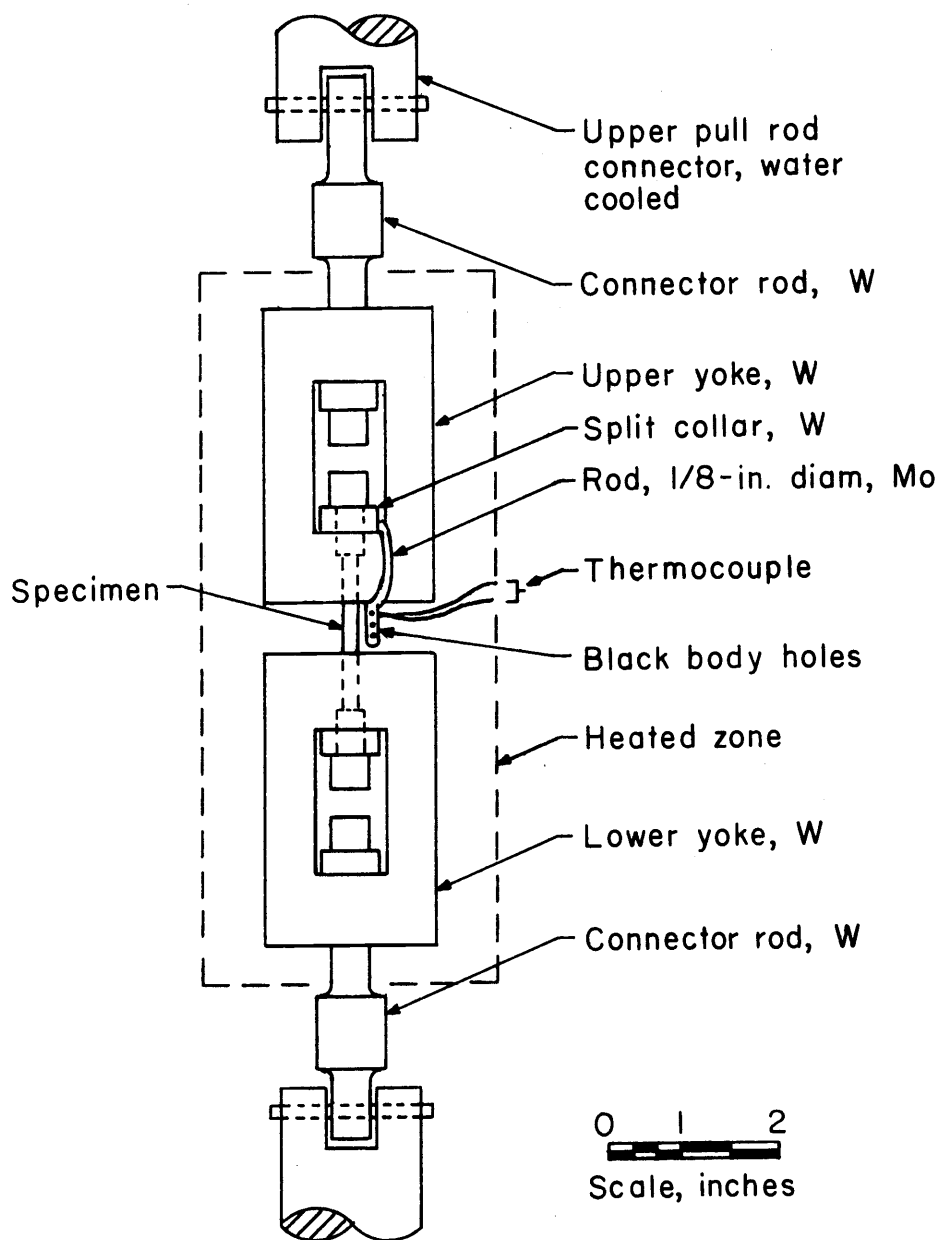
FIGURE 3.- Creep Specimen, Load Train,
and Thermocouple.

72-78

inch diameter, was located in one of the holes. The other three black body holes were used for optical pyrometer observations.

Temperature control was within ± 2°C over a period of days, and for many creep runs was within ± 1°C as measured by thermocouple. Agreement between the thermocouple and pyrometer temperature measurements, after making the required corrections, was frequently within 1°C and seldom beyond 5°C.

The change in length of the creep specimen was measured with an extensometer connected to the pull rods just outside of the vacuum chamber. A 40-inch quartz push rod exposed to room air activated the LVDT (linear variable differential transformer) which provided a signal for a chart recorder. The amplification factor between the specimen extension and the chart pen displacement was 200. Changes in ambient temperature could affect the extensometer measurements because of thermal expansion. However, the constant temperature of the water cooled furnace jacket and pull rods combined with the low expansivity of the quartz rod allowed room temperature variations of 3 to 5°C without causing a problem. The extensometer system was calibrated with a high precision micrometer graduated directly in 0.0001 inch. The AEC 77/ showed that the error caused by measuring the extension of the load train instead of the actual gage section of a creep specimen is small and is linear with extension.

Metallography

Typical specimens were examined by optical and electron microscopy to determine the grain size and shape of the tungsten phase and the size and spacing of the ZrO_2 particles. The stability of the microstructure during creep testing was also observed.

Specimens were sectioned with a diamond cut-off saw. The samples were mounted in bakelite and ground and polished by standard methods through 1/4-inch micron diamond. To reveal the tungsten grain boundaries for the optical microscope, an etch-polish with 4% chromic acid was used with Fe_2O_3 abrasive.

Specimens were prepared for 2-stage replication by an additional etching with a solution of 15 parts lactic, 5 parts nitric, and 5 parts hydrofluoric acid. The 2-stage replication method utilized a plastic replica followed by a carbon replica which was examined in the electron microscope. Resolution was limited to about 200A.

From samples of eight specimens, ZrO_2 particles were extracted and observed directly by electron microscopy in order more accurately to determine the particle size and spacing. The samples were first electro-polished in a 6 pct aqueous solution of Na_3PO_4 at 8 volts with a current density of 0.2 amp per cm^2. After evaporating a film of carbon onto the polished surface, the particles were released by dissolution of the tungsten matrix in an aqueous solution of 1 pct H_2O_2. Six of these samples were then shadowed with chromium in order to positively distinguish between very small ZrO_2 particles and etch pits. The extracted

ZrO_2 particles were also identified by X-ray diffraction in a Debye-Sherrer camera.

III.   RESULTS AND DISCUSSION

Development and Stability of the Microstructure

A satisfactory heat treatment was found to be an aging treatment of 20 hours at 1800°C. This treatment produced a relatively dense dispersion of submicron ZrO_2 particles in both Alloy I and II. Typical microstructures of the aged alloys are shown in Figure 4 and 5. To check the stability of the dispersoid, the alloys were heated for an additional 60 hours at 1800°C which was above the temperatures selected for creep studies. The dispersoid and the grain size of the tungsten matrix were found quite stable, as can be seen in Figure 6 after the 80 hour treatment at 1800°C. The grain size of the tungsten matrix and the size of the ZrO_2 particles are not significantly larger after the 80-hour treatment. Thus, the structure could be expected to remain quite stable during creep testing at temperatures below 1800°C.

Microstructures were also observed after creep testing to verify the stability of the grain size and ZrO_2 particle size. Figure 7 shows the microstructure after rather extreme testing, namely, 88 hours at 1630° to 1792°C plus 6 hours at 1924°C with stresses of 10,000 and 5,000 psi. The microstructure reveals very fine particles of less than 0.1 micron diameter that remained after testing. Larger ZrO_2 particles also remained but were not included in this particular photomicrograph.
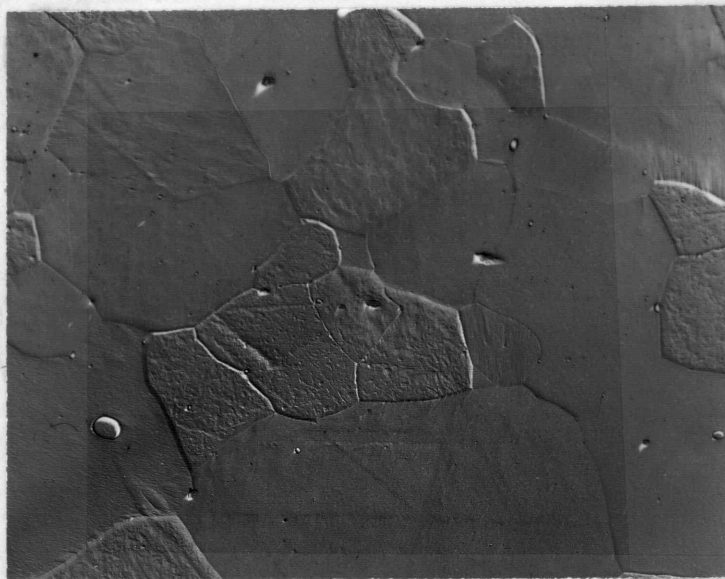
2700X
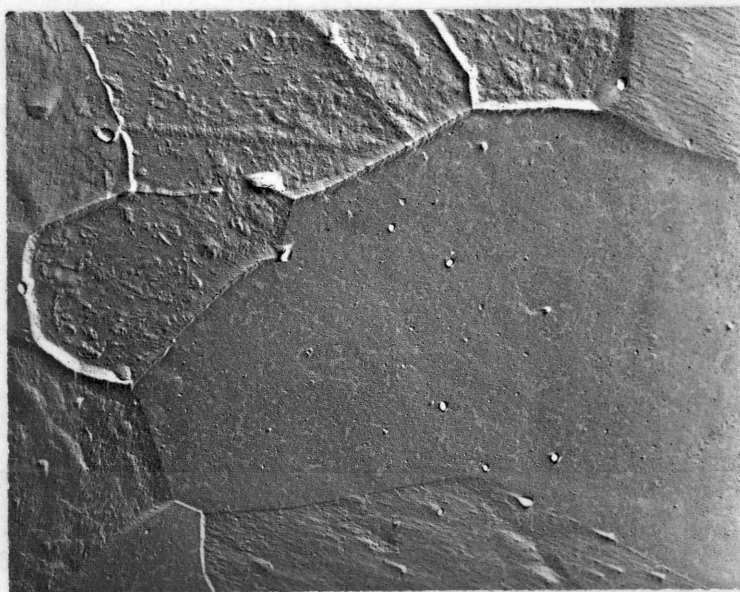
7500X

Figure 4. Microstructure of Type I alloy before testing. ZOW 17, heat treated 20 hr. at 1800°C. Etched, two stage plastic-carbon replicas. Light colored particles are ZrO_2. The extremely fine texture is the etch pit character of the W matrix.
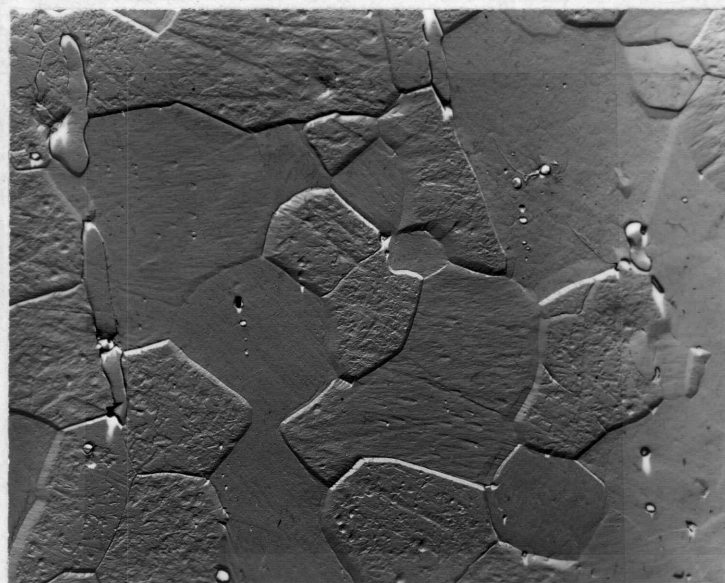
2700X
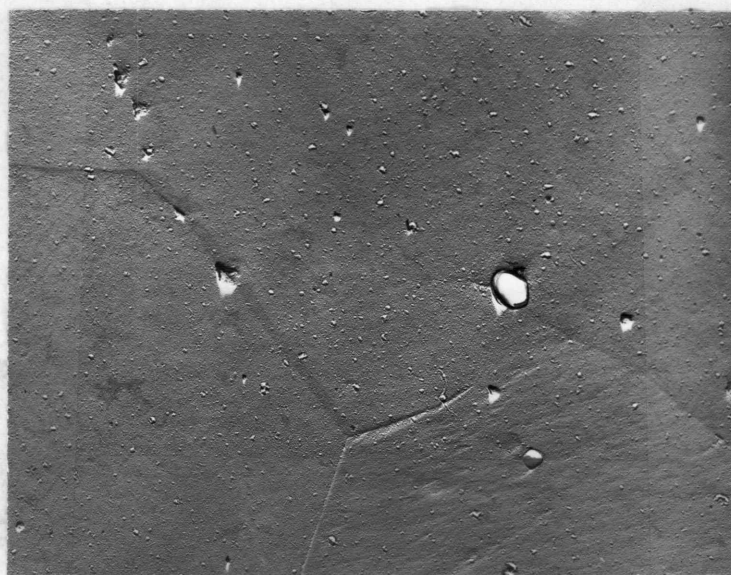
7500X

Figure 5. Microstructure of Type II alloys before testing. ZOW 24, heat treated 20 hr. at 1800°C. Etched, two stage plastic-carbon replicas. Light colored particles are ZrO_2. The extremely fine texture is the etch pit character of the W matrix.
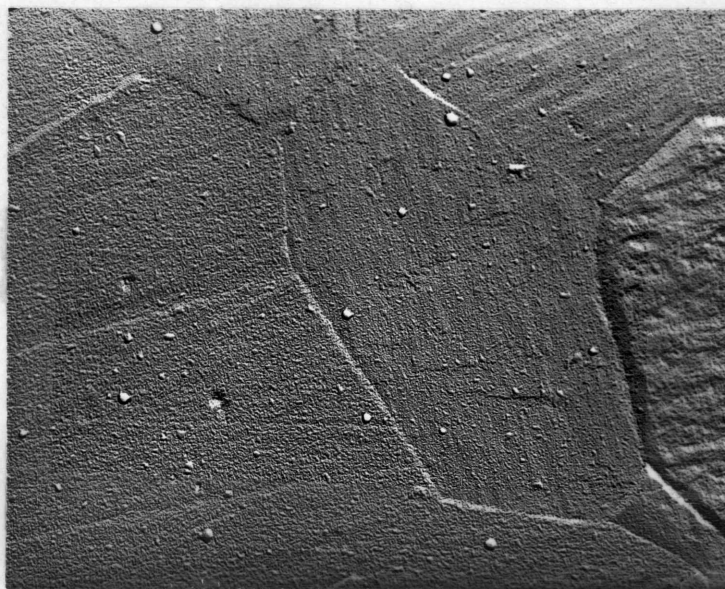
7500X

Figure 6. Microstructure of Type II alloy over-aged. ZOW 24, heat treated 80 hr. at 1800°C. Etched, two stage plastic-carbon replica. The light colored particles are ZrO_2. The fine texture is the etch pit character of the W matrix.

21,000X
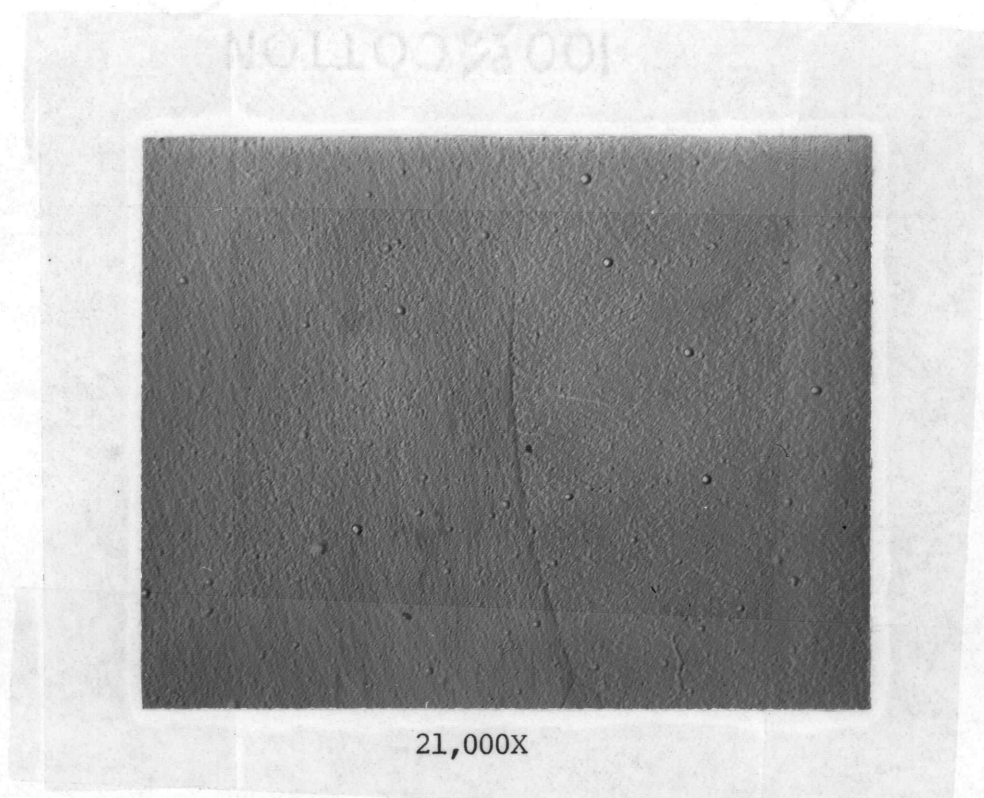
Figure 7. Microstructure of Type II alloy after testing. ZOW 28B, creep tested 96 hr. at 1630 to 1924°C. Structure retained even the very fine ZrO_2 particles. Etched, two stage plastic-carbon replica.

Microstructural Features

Grain size

The size of the grains in the tungsten matrix was determined from
the mean intercept length in a plane. The results are tabulated in
Table III. In the initial heat treated condition, the mean intercept
length in Type I and Type II alloy was 5.8 and 6.2 micron respectively.
The grains were equiaxed. The overaging treatment of 80 hours at 1800°C
produced only a slight increase in grain size, namely to about 6.8 and
8.2 microns respectively for Type I and II alloys. Long periods of
creep testing also increased the grain size slightly as seen from the
data of Table III.

Particle Size and Spacing

An optimum particle size and spacing exists for providing the
maximum strengthening effect in a dispersion strengthened alloy. Par-
ticles which are too small will be incapable of blocking a dislocation.
The spacing of the particles affects the stress at which the dislocation
will bow between the particles and break away. McLean [46] gives an
optimum particle spacing of about 2 to 20 x 10^2 atomic diameters which
for tungsten is from about 6 to 60 x 10^{-6} cm or 0.06 to 0.6 micron.

The results of the particle size and spacing determinations of
the ZOW alloys are summarized in Table III. It was difficult to dis-
tinguish between very fine ZrO_2 particles and etch pits in the 2-stage
replicas. The shadowed extraction replicas make the distinction very

clear because the shadows are in opposite direction in the two cases.
The extraction replicas have the additional advantage of revealing the
true size of the particles rather than a random planar section [8/].
Typical microstructures of extraction replicas of the ZOW alloys Type
I and II are shown in Figure 8 and 9, respectively.

Most of the particles in Type I and II specimens fell within the
size range of 0.05 to 0.5 micron with the mean diameter estimated as
0.2 micron or 2×10^{-5} cm and used in later calculations. The particle
size data are included in Table III. The few very large particles in
the 4 to 8 micron size range, which are typical of all the ZOW alloys,
were not counted. Type II specimens contained at least two times the
density of the large particles as Type I.

The mean spacing between the ZrO_2 particles, λ, was determined by
counting the particles within a given measured area on three represen-
tative photographs of extraction replicas of each specimen listed.
From Table III, the values of mean particle spacing, determined from
the extraction replicas, ranged from 1.5 to 2.0 microns except for speci-
men 28 with $\lambda = 3.3$ microns. The values seen in Table II indicate no
difference in mean particle spacing between Type I and II alloys. A re-
asonable value for λ was taken as 2 micron, and used in later calculations.

Tensile Tests

The results of the tensile tests are best seen by referring to
Figure 10 and to the data in Table IV. Both the ultimate tensile
strength and the 0.2% offset yield strength were slightly greater for
the Type I alloy. At test temperatures of 1800°C and above, a true
yield point phenomenon was observed in the stress-strain curves. In-
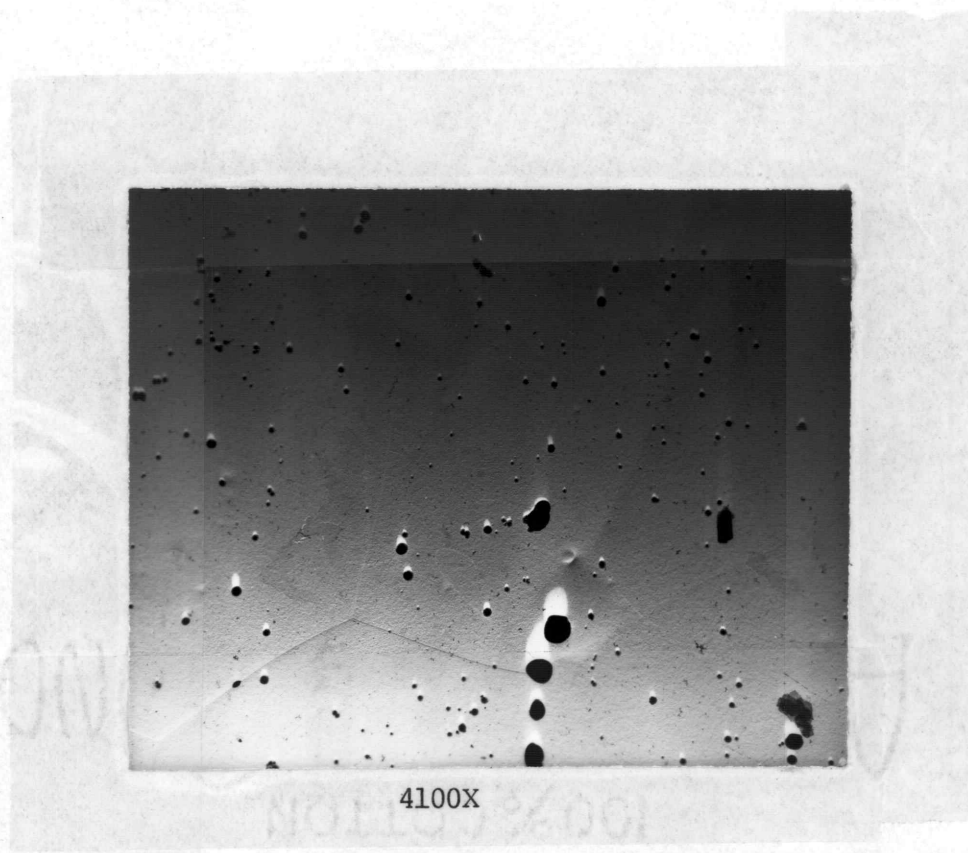
4100X

Figure 8. Extracted particles of Type I alloy after creep testing.
ZOW 17A, carbon extraction with shadowing. Black par-
ticles are ZrO_2. Light areas are shadows.
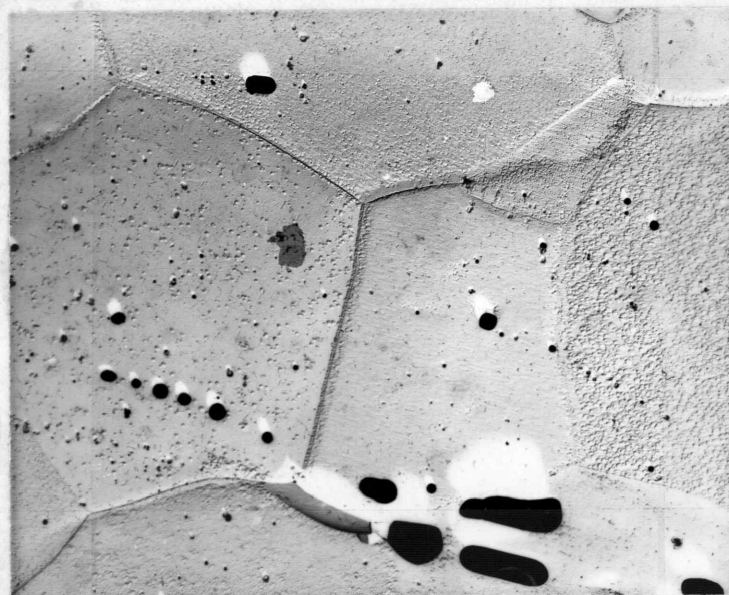
4100X

Figure 9. Extracted particles of Type II alloy after creep testing.
ZOW 28A. Carbon extraction with shadowing. Black par-
ticles are ZrO_2. Light areas are shadows. Etch pits are
distinguished from particles by opposite direction of
shadow.

Table III. Estimates of particle size and spacing of ZOW specimens

2 stage replicas

Alloy type	ZOW No.	Condition and history [1]	Dia, h, micron	Mean [2] spacing λ, micron	Grain, [3] $\Delta\ell$, micron
I	17	H.T. 20h @ 1800°C	.05–.5	.5	5.4 } 5.8
I	23	H.T. 20h @ 1800°C	.05–.5	.5	6.2
II	24	H.T. 20h @ 1800°C	.05–.5	.5	5.6 } 6.2
II	28	H.T. 20h @ 1800°C	.05–.5	.5	6.8
I	23	H.T. 80h @ 1800°C	.1 –.5	1	6.8
II	24	H.T. 80h @ 1800°C	.1 –.5	1	8.2
I	18A	H.T. 20h, creep tested, 1801°C	.05–.5	1	–
I	18B	H.T. 20h, creep tested, 1782°C	.05–.5	2	–
I	22A	H.T. 20h, creep tested, 1620°C	.05–.5	2	–
II	28A	H.T. 20h, creep tested, 1632°C	.1 –.5	1	–
II	28B	H.T. 20h, creep tested, 1924°C	.1 – 1	1	–

Extraction replicas

Alloy type	ZOW No.	Condition and history [1]	Dia, h, micron	Mean [2] spacing λ, micron	Grain, [3] $\Delta\ell$, micron
I	17	H.T. 20h @ 1800°C	.05–.5	1.9	6.0
II	28	H.T. 20h @ 1800°C	.05–.5	3.3	8.6
I	17A	H.T. 20h, creep tested, 1573°C	.05–.5	1.5	8.5
I	18A	H.T. 20h, creep tested, 1801°C	.05–.5	2.0	9.1
II	28A	H.T. 20h, creep tested, 1632°C	.05–.5	1.7	9.0

[1] Temperature is given for only the last run of several runs during creep tests.

[2] Mean spacing in a random planar section.

[3] $\Delta\ell$ = mean intercept length in a plane.

Table IV. Tesile test data of ZOW alloys tested under vacuum

Alloy type	ZOW No.	Test temp., °C	Tensile strength, kpsi	0.2% offset yield, kpsi	Elongation in 1-inch pct	Reduction in area, pct
I	21	1600	45.7	28.4	14	20
II	26A	1600	44.1	30.9	9	12
I	33A	1700	31.4	25.1	11	18
I	34A	1800	29.0	27.3	14	27
II	36A	1900	26.4	26.4	10	16
II	37A	2000	24.4	24.4	8	16
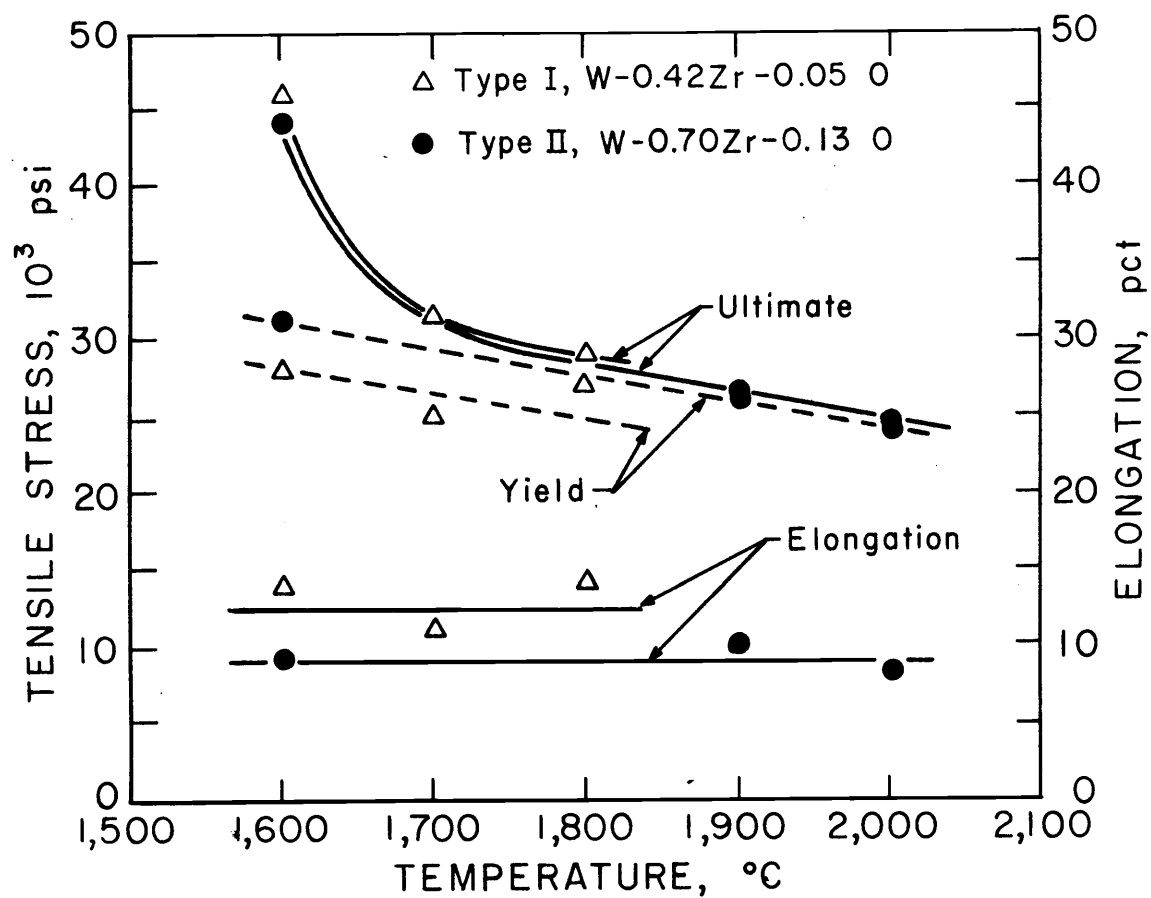
FIGURE 10.- Tensile Data of ZOW Alloys,
Aged 20 hr at 1,800° C.

71-270

terestingly, the true yield point agreed exactly with the 0.2% offset

yield strength. The elongation ranged from 8 to 14 percent and the

reduction in area ranged from about 12 to 27 percent. The comparative

yield strength of these alloys and several other tungsten alloys are

shown in Figure 11.

Stress-rupture

The eight stress-rupture tests were carried out at two tempera-

tures, 0.547 T_{mp} (1740°C) and 0.448 T_{mp} (1375°C) over a stress range

of 10,000 psi to 60,000 psi. The resulting lifetimes ranged from 1.43

to 190 hours. The stress-rupture data are given in Table V; the plots

of stress versus time to rupture are shown in Figure 12. The test

temperatures are only approximate because these tests were performed

during the early stages of the testing program when the furnace was

controlled by a transducer rather than the thermocouple.

For comparison, the stress-rupture lives of unalloyed tungsten

and several other tungsten alloys at a temperature of 1650°C (3000°F)

are shown in Figure 13. The curve for the aged ZOW alloys was obtained

by interpolation of the data in Figure 12 with the aid of the exponen-

tial relation commonly used in which the lifetime is proportional to

e^{-Q}/RT. Q is the activation energy for creep which was taken as

104,200 cal per mole deg (as discussed later), and T is the absolute

temperature. The resulting curve is seen to lie very close to the ex-

perimental curve for ZOW alloys in the as-extruded condition [11/].

The stress-rupture life of the ZOW alloys is appreciably longer than

that of commercial thoria dispersed tungsten and W-10 vol pct HfO_2
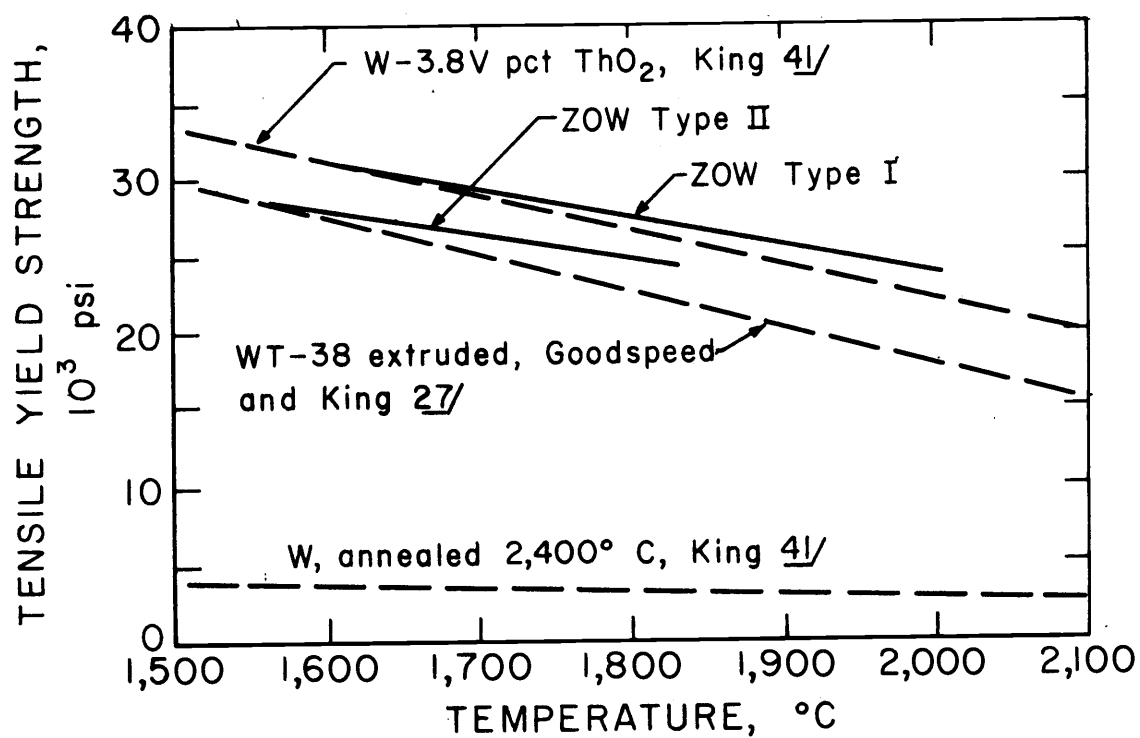
FIGURE II.-Comparative Tensile Yield Strength of
Tungsten and Tungsten Alloys.

71-269

Table V. Stress-rupture data for the ZOW alloys aged 20 hr at 1800°C

Alloy type	ZOW No.	Temp., °C	Stress, psi	Life, hr	Elong., pct	Reduction area, pct
I	20A	1379	30,360	189.8	11	12
I	20B	1368	60,000	1.43	19	30
I	19A	1739	10,360	45.3	9	10
I	19B	1735	20,360	2.5	11	16
II	25A	Erratic	34,000	3.8	10	14
II	26B	1375	34,000	120.8	8	12
II	27A	1382	50,000	4.0	11	13
II	24	1743	10,000	46.3	8	7
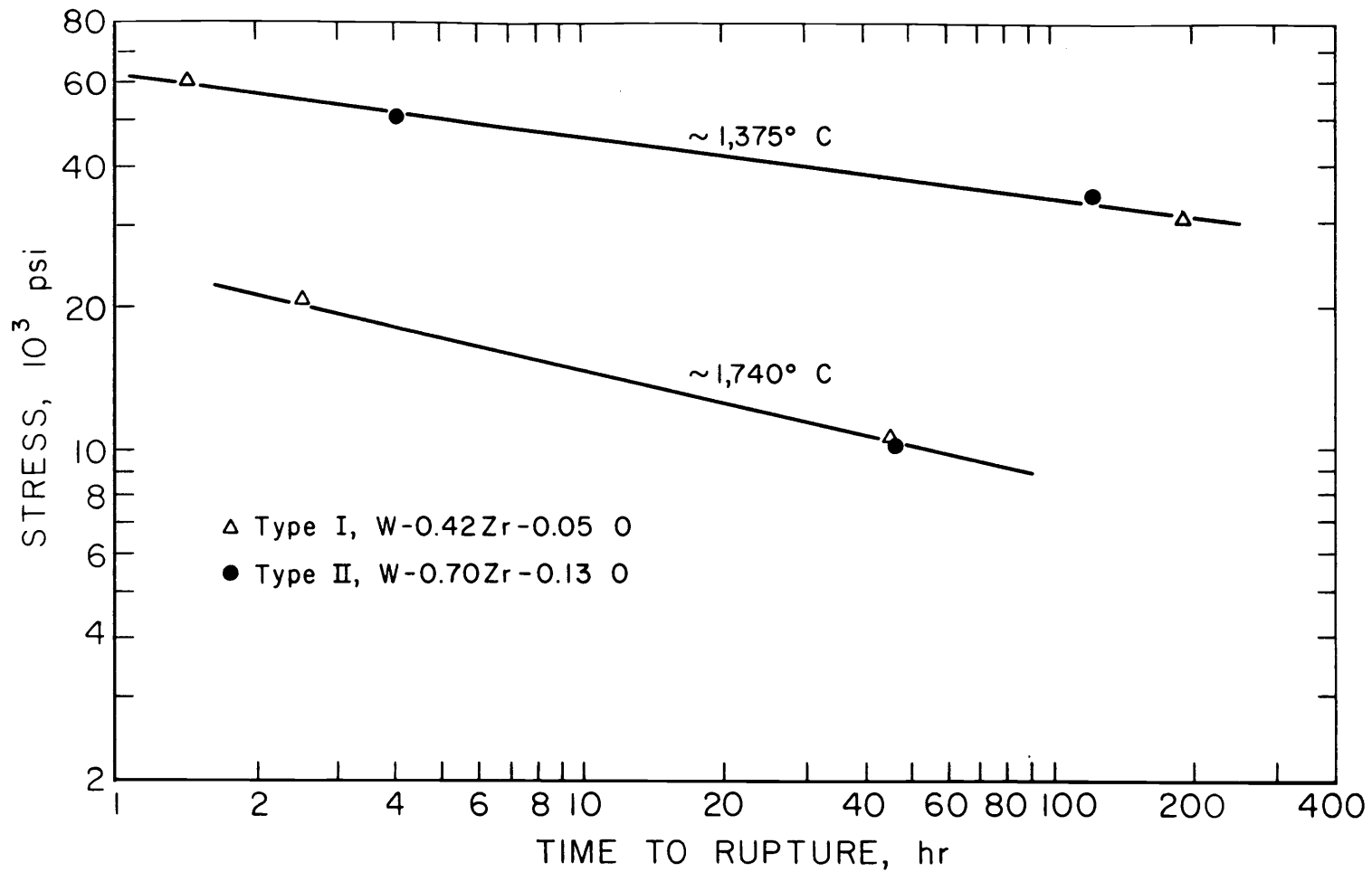
FIGURE 12.-Stress-Rupture Life of ZOW Alloys, Aged 20 hr at 1,800° C.

71-274
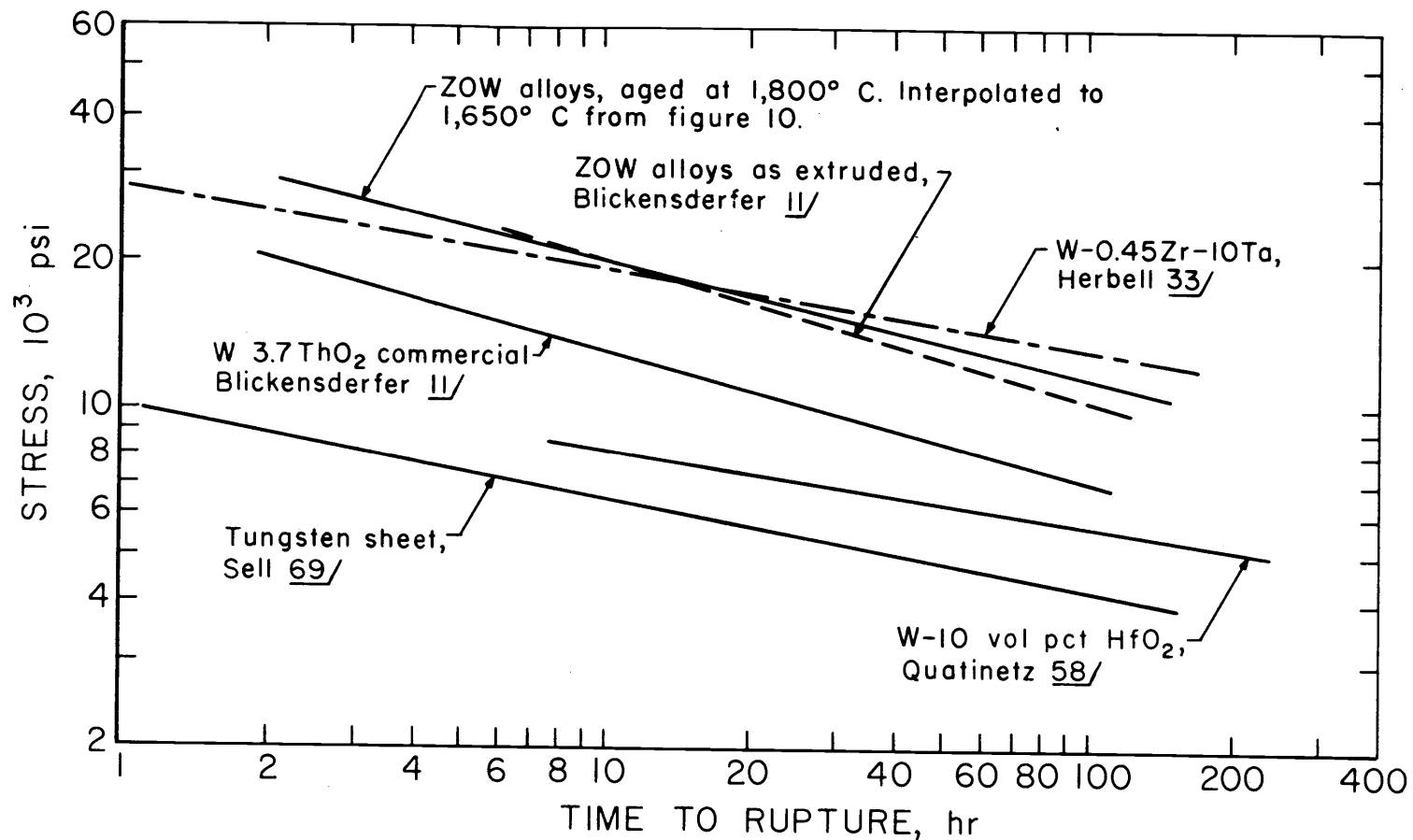
FIGURE 13.-Comparison of Stress Rupture Life of Tungsten and Tungsten Alloys at 1,650° C (3,000° F).

produced by Quatinetz [58/]. The ZOW alloys are comparable to the best alloy tested by Herbell [33/], W-0.45 Zr-10Ta.

Creep

The steady state creep rate was measured over a temperature range of 1465° to 1924°C and a stress range of 3,500 to 20,000 psi. Appendix I gives the experimental values obtained for strain rate on all of the 61 runs. Each run was at a constant applied load and temperature. Most runs lasted from about 3 to 40 hours; the longest run was 93 hours. The strain rates ranged from 5.6×10^{-9} to 1.08×10^{-6} per second. Appendix I does not include an additional 23 preliminary runs for determining suitable ranges of stress and temperature used to establish and refine experimental technique. Several runs were attempted during which the stress was cycled by $\Delta\sigma$ or the temperature was cycled by ΔT. But, because of the relatively long times required to reach steady state creep after each change, this testing procedure was discontinued.

Some of the data listed in Appendix I were declared invalid because of problems with temperature control or thermocouple failures. A few data were discarded because the specimen entered stage III creep or because the steady state creep rate was definitely too high in comparison with other data in a plot of ln $\dot{\varepsilon}$ vs 1/T. The two runs on ZOW 35B and the last four runs on ZOW 22A were in the latter category.

The dimensions of the creep specimens, reduction in area, and elongation are given in Appendix II. The reduction in area data were used to correct the nominal stress to true stress. The corrections were

calculated after the completion of all runs on the specimen by pro-
rating the reduction in area in proportion to the amount of total strain
at the midpoint of each given run. In most runs the stress correction
was less than one percent, the maximum being three percent.

A comparison of the creep rates of tungsten and several tungsten
alloys at a temperature of 1,650° (3,000°F) is given in Figure 14. The
low creep rates of the ZOW alloys make them superior to the other alloys
for which data are available. The strain rate is about three orders of
magnitude lower than unalloyed tungsten. The strain rates of the HfC
dispersion strengthened tungsten alloys of Raffo and Klopp [60/] were re-
ported at 1920°C. A test of ZOW alloy Type II, at 1924°C and 5,000 psi
stress, gave a creep rate about 10 times greater than the best alloy of
Raffo and Klopp, W-0.20Hf-0.26C; however, extrapolation of the data for
ZOW alloys at 10,000 psi indicates a strain rate about 5 times less than
the above HfC strengthened alloy.

Activation Energy

The steady state creep data which were used for the determination
of the activation energy of creep are tabulated in Table VI. Data were
limited to temperatures below about 1800°C where the microstructure re-
mained stable. The creep rates are corrected for the increase in stress
caused by the reduction in area as the test progressed. This correction
of $\dot{\epsilon}$ was obtained with the aid of a preliminary graph of ln $\dot{\epsilon}$ vs σ. By
applying the correction, the data for activation energy are at constant
true stress rather than engineering stress.
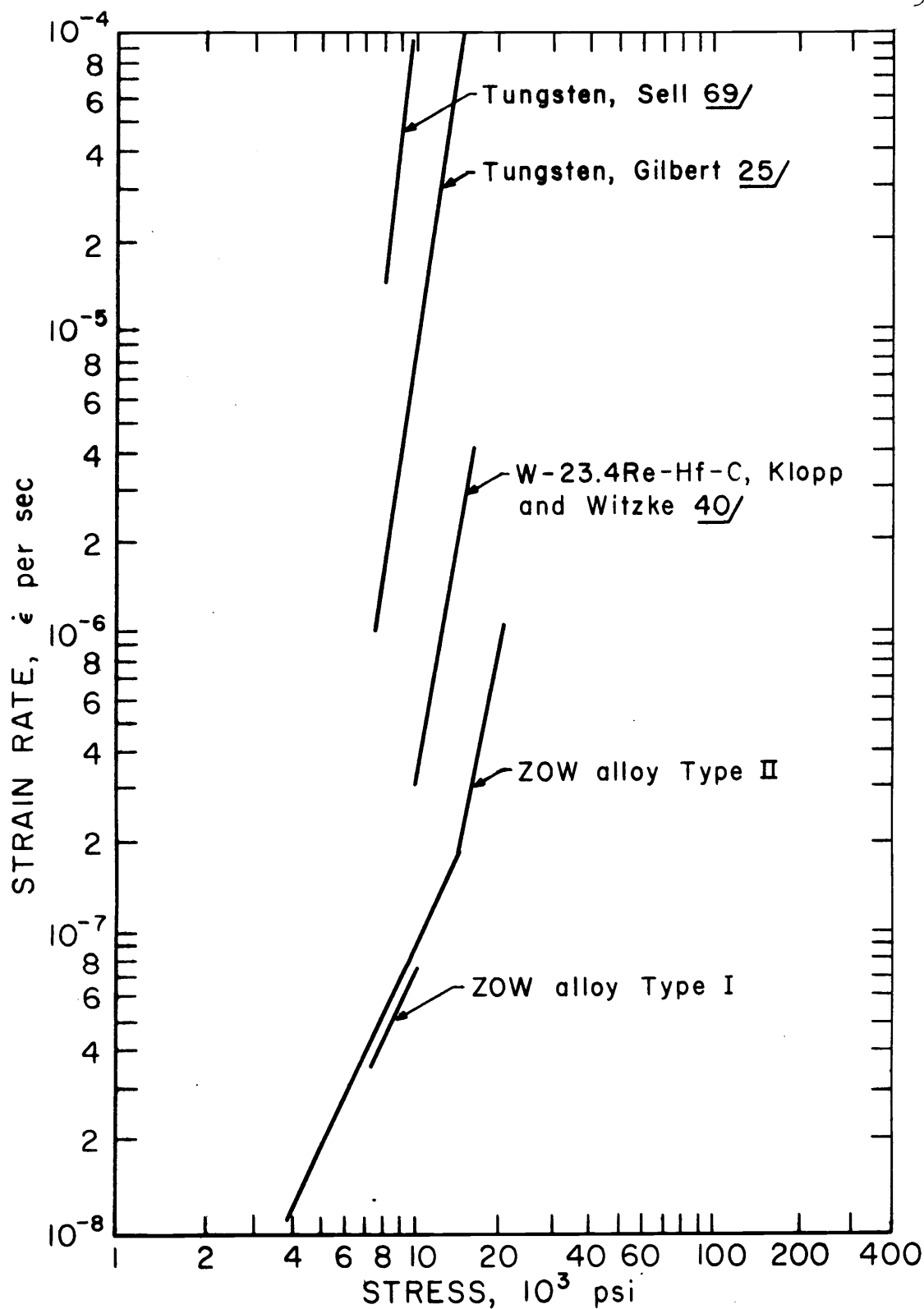
FIGURE 14.—Comparative Relation of $\dot{\epsilon}$ and σ for Tungsten Alloys at 1,650° C (3,000° F).

71-272

Table VI. Steady-state creep data

Alloy type	ZOW No.	Run No.	Nominal stress σ, psi	Reduction in area,[1] pct	Corrected $\dot{\varepsilon}$, per second	Temperature, °C
I	18B	3	7,200	1.0	1.07×10^{-7}	1742
I	22A	1	7,200	0.1	2.27×10^{-8}	1618
I	17A	5	10,000	2.0	5.14×10^{-7}	1808
I	18A	2	10,000	0.3	1.66×10^{-8}	1545
I	18A	3	10,000	0.5	5.78×10^{-8}	1632
I	18A	4	10,000	0.8	1.07×10^{-7}	1687
I	18A	5	10,000	1.2	5.48×10^{-7}	1801
I	18B	1	10,000	0.1	2.55×10^{-8}	1578
I	18B	2	10,000	0.6	2.60×10^{-7}	1742
II	29B	3	3,500	0.9	5.65×10^{-9}	1511
II	29B	4	3,500	1.2	7.16×10^{-8}	1801
II	28B	2	5,000	0.3	1.16×10^{-8}	1626
II	28B	3	5,000	0.6	1.05×10^{-7}	1792
II	28B	4	5,000	0.7	3.18×10^{-8}	1701
II	27B	3	7,200	1.5	1.57×10^{-7}	1741
II	27B	4	7,200	2.2	8.04×10^{-8}	1684
II	27B	5	7,200	2.6	4.04×10^{-8}	1626
II	27B	6	7,200	3.0	3.27×10^{-7}	1791
II	29A	1	7,200	0.1	2.01×10^{-8}	1582
II	27B	1	10,000	0.2	2.97×10^{-8}	1570
II	27B	2	10,000	0.7	3.03×10^{-7}	1740
II	28A	1	10,000	0.2	3.60×10^{-8}	1580
II	28B	1	10,000	0.1	6.05×10^{-8}	1629
II	29A	3	10,000	1.5	1.20×10^{-7}	1671
II	29B	1	14,000	0.1	2.35×10^{-8}	1511
II	29B	2	14,000	0.6	2.47×10^{-7}	1671
II	28A	2	20,000	0.6	3.96×10^{-7}	1582
II	28A	3	20,000	1.1	1.74×10^{-7}	1534
II	28A	4	20,000	1.3	5.55×10^{-8}	1465
II	29A	2	20,000	0.7	7.03×10^{-7}	1630

[1] Calculated total reduction in area at mid point of run based on the total reduction in area at completion of all runs on the specimen.

The activation energy for steady state creep was determined from each of two basic relationships on a thermally activated process

$$\dot{\varepsilon} = A \ f \ (\sigma) \ \exp \ (\frac{-Q}{RT}) \qquad\qquad [1]$$

and $\dot{\varepsilon} = A \ \frac{f \ (\sigma)}{T} \ \exp \ (\frac{-Q}{RT}) \qquad\qquad [2]$

At constant stress these equations reduce respectively to

$$\dot{\varepsilon} = A \ \exp \ (\frac{-Q}{RT}) \qquad\qquad [3]$$

and $\dot{\varepsilon}T = A \ \exp \ (\frac{-Q}{RT}) \qquad\qquad [4]$

The corrected values of $\dot{\varepsilon}$ were plotted according to the relations of equations [3] and [4]. In both cases the activation energy was essentially constant over the range of temperature and stress. Figure 15 shows the curves for the plot of log $(\dot{\varepsilon}T)$ vs $\frac{1}{T}$ (equation [4]). The lines shown for each stress level and alloy type are the best fit according to linear regression analysis. The values of the slope, m, and the standard deviation determined by the linear regression analyses are given in Table VII.

The mean value of the slope, m, was calculated from the mean of all values weighed in proportion to the number of data points corresponding to each value of m. This mean value of m was $-2.278 \times 10^4 \pm 0.069 \times 10^4$ which yields an activation energy $Q = 104,200 \pm 3,200$ cal per mole °K. The slope or activation energy of type I alloy did not differ significantly from type II alloy even though type I alloy possessed lower creep rates.
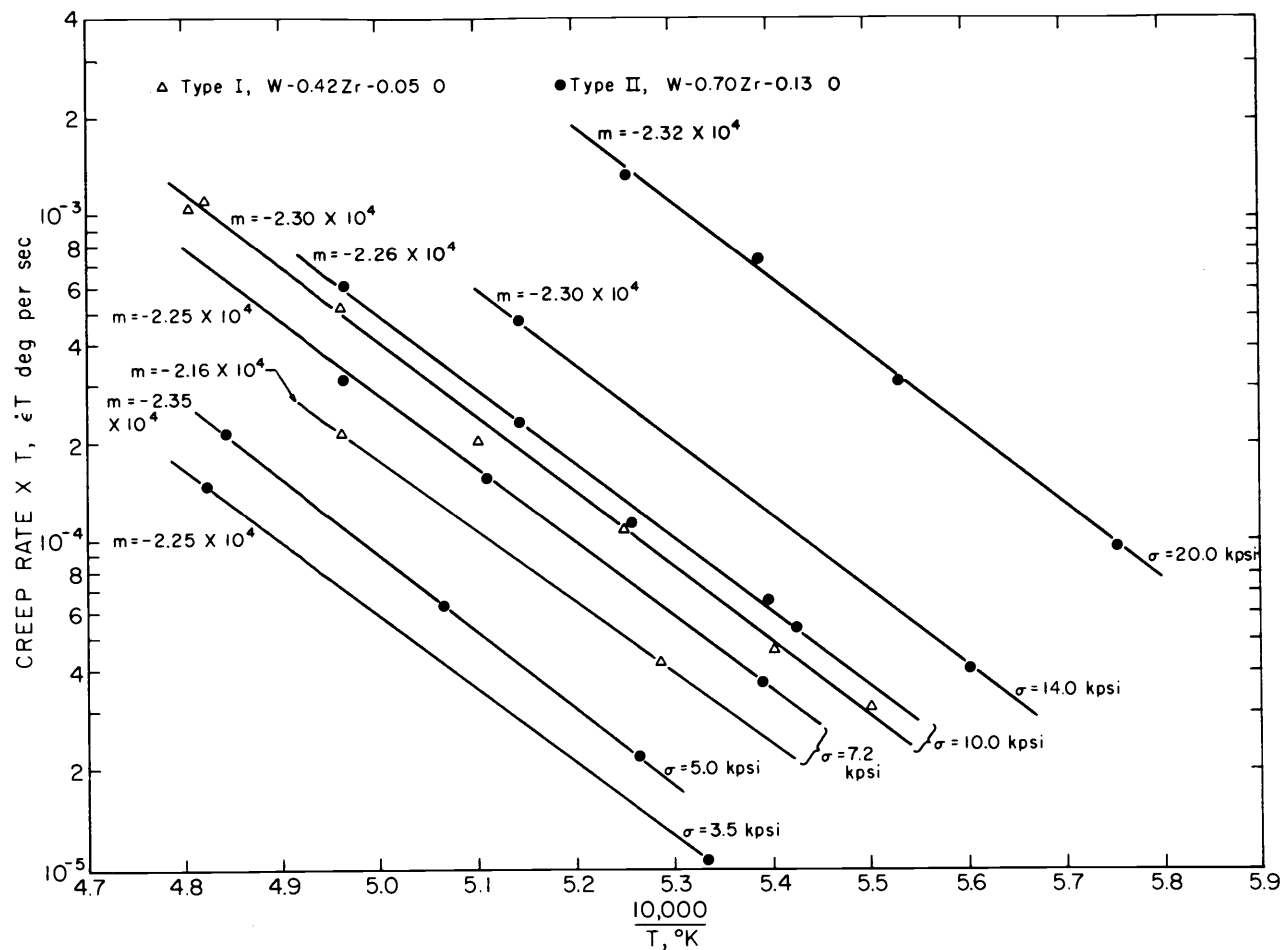
FIGURE 15.-Relation Between Steady State Creep Rate, $\dot{\epsilon}$, and Temperature. ZOW alloys, aged 20 hr at 1,800° C. The mean value of the slope, m, is -2.278 X 10^4 for a Q of 104,200 cal per mole deg.

71-268X

Table VII. Calculated slopes,m, of curves

$$\log(\dot{\epsilon}T) = m\left(\frac{1}{T}\right) + b$$

Alloy type	σ, psi	Slope, 10^4 °K	
		m	± std. dev.
I	7,200	−2.157	[1]
	10,000	−2.295	0.053
II	3,500	−2.253	[1]
	5,000	−2.351	0.039
	7,200	−2.245	0.070
	10,000	−2.262	0.092
	14,000	−2.297	[1]
	20,000	−2.320	0.078

[1] Not defined for only 2 data points

The analysis of the data according to equation [3] was carried out and provided the same conclusions as discussed above. The mean slope was -2.202 x 10^4 which gave a Q = 100,700 cal per mole °K. Because the relation of equation [3] did not provide quite as good a fit to the data by linear regression analyses and since equation [4] is more amenable to a theoretical derivation, the former value Q = 104,200 cal per mole °K was accepted.

Stress Dependence of the Strain Rate

From the previous discussion it is seen that the activation energy was independent of stress as well as temperature over the range discussed. Because the curves of the log ($\dot{\varepsilon}$T) vs 1/T data are parallel, a constant relationship between stress and $\dot{\varepsilon}$ exists for any given temperature. That is, for a given temperature, the intervals between the stress curves of Figure 15 are essentially the same as for another temperature. If all of the slopes were corrected to the mean value of -2.278 x 10^4, the relation between $\dot{\varepsilon}$ and stress would be the same for any temperature.

The slopes of the log ($\dot{\varepsilon}$T) vs 1/T curves of Figure 15 were corrected to -2.278 x 10 in the following manner. Each curve was rotated about its midpoint to a slope of -2.278 x 10^4. The midpoint was for the value of temperature which was the mean of the data points for the given curve. The original intercept which was calculated from the linear regression analysis was then corrected to b_c to satisfy the new slope of -2.278 x 10^4. Thus the new equations of the curves were of the form

$$\log (\dot{\varepsilon}T) = \frac{-2.278 \times 10^4}{T} + b_c \qquad [5]$$

with only the values of b_c being different for the different curves.

A temperature of 1618°C was chosen for analyzing the stress dependence because it included creep rate data over the full range of stresses from 3,500 to 20,000 psi. Direct measurement of strain rate over a range of stresses at a constant temperature of 1618°C were obtained directly on specimen ZOW 36C, type II. These data, along with the calculated values of $\dot{\varepsilon}$ discussed above on specimens of type II alloy, are tabulated in Table VIII. The agreement is quite good with all of the direct measurements of $\dot{\varepsilon}$ slightly greater than the calculated values at a given stress. The calculated points and the experimental points from ZOW 36C are plotted in Figures 16, 17, and 18. The straight line portion of the curves was used to establish the functional relation between stress and strain rate.

A number of relations have been proposed for the stress dependence of $\dot{\varepsilon}$ in dispersion strengthened materials. All models assume that some aspect of glide dislocation mobility, such as the rate of generation of dislocations at sources or the rate of particle bypass, is so slow as to become rate controlling for steady state creep [3]. Ansell and Weertman [6] derived equations for creep rate which varied as σ at low stresses and as σ^4 at higher stresses. Following Schoek [64] they assumed that the rate controlling process was the climb of dislocations over the dispersed particles. However, the same author's work on dispersion strengthened aluminum alloys suggested an exponential equation of the form

$$\dot{\varepsilon} = C \exp \left(\frac{B\sigma}{kT} \right) \qquad [6]$$

Table VIII. Steady-state creep rates at 1618°C, type II alloy

Stress, psi	Calculated from $\dot{\varepsilon}$ vs 1/T data	Run No.	Specimen ZOW 36C
3,500	6.89×10^{-9}	–	–
5,000	1.06×10^{-8}	6	1.10×10^{-8}
7,200	3.35×10^{-8}	1	4.26×10^{-8}
10,000	5.78×10^{-8}	2	6.47×10^{-8}
	–	5	6.12×10^{-8}
12,000	–	9	8.70×10^{-8}
14,000	1.17×10^{-7}	7	1.42×10^{-7}
16,000	–	3	2.72×10^{-7}
20,000	6.14×10^{-7}	4	7.37×10^{-7}
	–	8	7.95×10^{-7}
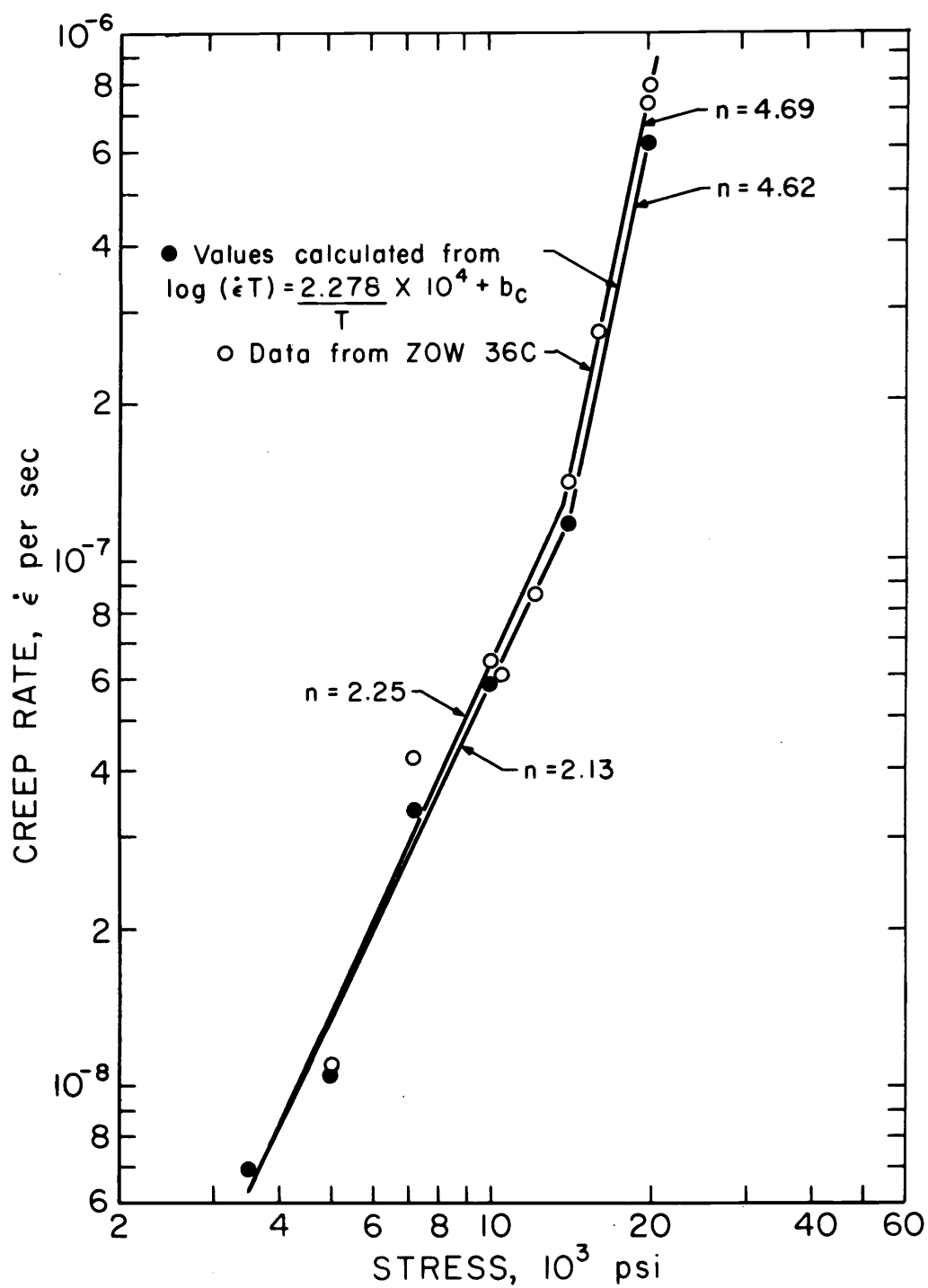
FIGURE 16.-Log Stress Versus Log $\dot{\epsilon}$ at 1,618° C.

71-267

CREEP RATE, $\dot{\epsilon}$ per sec

10^{-6}

Slope B = 1.11 X 10^{-4} per psi
○ Data from ZOW 36C

Slope B = 1.14 X 10^{-4} per psi
● Values calculated from
$\log(\dot{\epsilon}T) = \dfrac{-2.278}{T} \times 10^{-4} + b_c$

10^{-7}

10^{-8}

STRESS, 10^3 psi
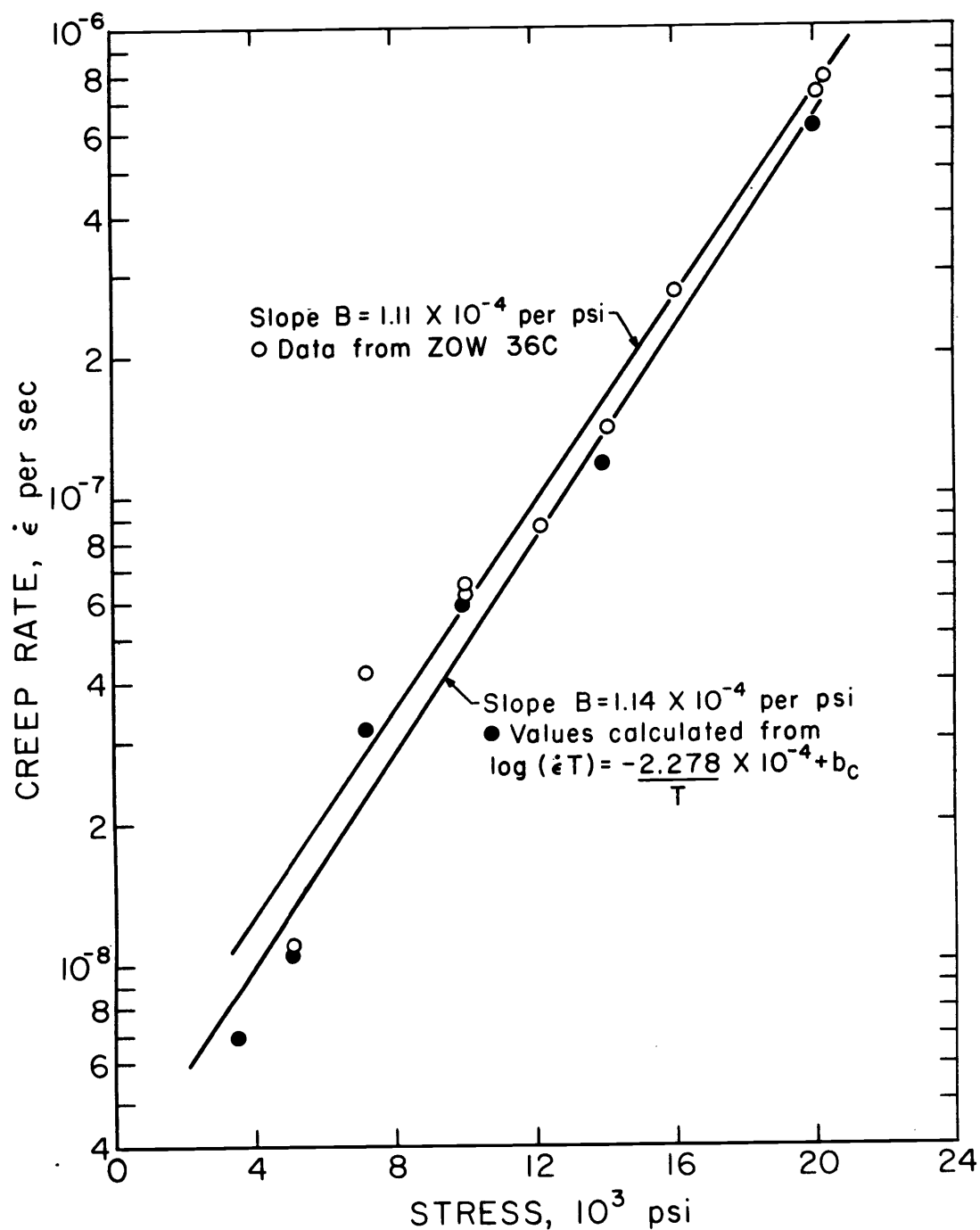
FIGURE 17.- Stress Versus Log $\dot{\epsilon}$ at 1,618° C.

71-266
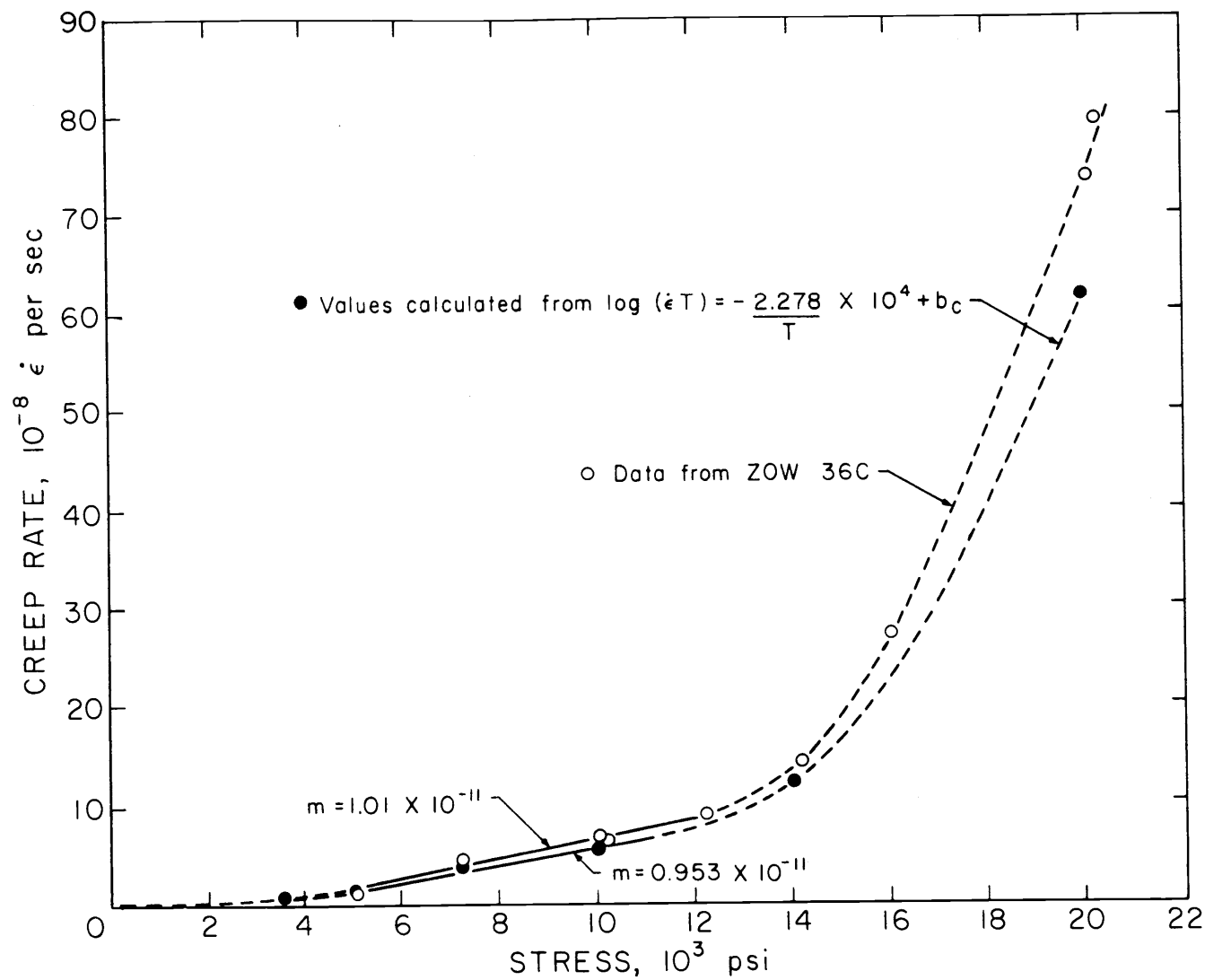
FIGURE 18.-Linear Plot of Stress Versus Creep Rate at 1,618° C.

The figure shows a plot with CREEP RATE, 10^{-8} $\dot{\epsilon}$ per sec on the y-axis (0 to 90) and STRESS, 10^3 psi on the x-axis (0 to 22).

● Values calculated from $\log (\dot{\epsilon} T) = -\dfrac{2.278 \times 10^4}{T} + b_c$

○ Data from ZOW 36C

$m = 1.01 \times 10^{-11}$

$m = 0.953 \times 10^{-11}$

71-271

Wilcon and Clauer [84], in studies of TD (thoria dispersed) nickel found

a dependency of stress on the activation energy for creep at temperatures

T <0.5 Tm such that

$$\dot{\varepsilon} = C \exp \frac{-Q(\sigma)}{RT} \qquad [7]$$

At temperatures T >0.5 Tm they found a power dependency upon the stress

of the form

$$\dot{\varepsilon} = C \sigma^n \qquad [8]$$

with n equal to about seven. Takahaski et al [75] in studies of nickel

strengthened with alumina found values of the stress exponent, n, equal

to 6.2 to 7.9. Chaudhuri [14], in a nickel base alloy, found both the

power and the exponential relations for stress satisfied reasonably well.

The power dependence was for n = 8.3. Ansell and Lenel [5] in a re-

crystallized SAP alloy found a power relation with the stress exponent,

n, equal to approximately four.

A linear dependency of stress on the creep rate

$$\dot{\varepsilon} = C \sigma \qquad [9]$$

has not been observed experimentally in dispersion strengthened alloys

although such viscous behavior is well known in diffusion controlled

creep such as Nabarro-Herring creep [34,46,53].

The author has attempted to find the best equation, [6], [7], [8],

or [9] compatible with a creep model for satisfying the experimental re-

sults. Equation [7] can be eliminated immediately because the activation

energy, Q, is not a function of stress, σ, as already shown by Figure 15.

Fits of the data of the remaining three equations were made by linear regression analyses in the appropriate coordinates.

Figure 16 shows a plot of log σ vs log $\dot{\varepsilon}$ for the points calculated from the 1/T vs log ($\dot{\varepsilon}$T) data and from the direct measurements on ZOW 36C. The slope n gives the exponent in the equation $\dot{\varepsilon} = C\sigma^n$. Two straight lines can be fit to each set of data points. In the low stress region the data points are scattered considerably; the average slope is about 2.2 In the region above the 14,000 psi stress the data points fit better and the slopes are 4.62 and 4.69 or average 4.66.

Figure 17 shows the same data on a semi log plot in an attempt to fit the equation

$$\dot{\varepsilon} = C \exp B\sigma.$$

The linear regression analyses gave slopes, B, of 110.9 per psi for the ZOW 36 data and 114.1 per psi for the calculated data. The fits are not particularly good. The data points at stresses of 14,000 psi and above fit fairly well to straight lines but not as well as in the preceding figure with the log σ vs log $\dot{\varepsilon}$ plot. One is tempted to ignore the data points 7,200 psi and 10,000 psi since the remaining points would give a good linear fit. However, the points at 7,200 and 10,000 psi were obtained from a total of 13 runs on five specimens and therefore cannot be dismissed.

Figure 18 shows a linear plot of the data points in an attempt to fit the relation $\dot{\varepsilon} = C\sigma$. The data fit straight lines quite well from 5,000 to 12,000 psi stress. Since these curves must pass through the origin, it appears that the straight lines break into curves at very low

stresses. At higher stresses, the straight lines curve upward abruptly above 12,000 psi.

It is concluded from Figures 16, 17, and 18 and the preceding discussion that the stress dependency of the steady state creep rate from 1500° to 1800°C should be explained by two functions rather than by a single simple mathematical expression. At low stresses, from about 5,000 to 12,000 psi, the strain rate varies linearly with the stress. At the higher stresses tested, from 14,000 to 20,000 psi, the logarithm of the strain rate varies with the logarithm of the stress to satisfy the equation

$$\dot{\varepsilon} = C^{\,n}$$

with n equal to about 4.6. A transition between the two types of stress dependency occurs from 12,000 to 14,000 psi stress.

Activation Volume

The activation volume was determined from the experimental data by use of the relation [30]

$$V^* = kT \left(\frac{\Delta \ln \dot{\varepsilon}}{\Delta \sigma} \right)_T \qquad [10]$$

The term in the bracket is 2.3 times the slope of the curve of Figure 17 of the plot of log $\dot{\varepsilon}$ vs σ. The activation volume is seen to increase linearly with temperature. At a temperature of 1618°C, the activation volume was calculated as 1.3×10^{-21} cm^3. This value is in good agreement with the work of Sell et al [70] who obtained values of 1.6 to 2.3×10^{-21} cm^3 for thoria dispersed tungsten, TDW-WHS, from 8 to 12 ksi at 2100°C.

Empirical Creep Equations

Upon inclusion of the temperature dependence and the activation energy as previously discussed, and after solving for the constants, the following two equations result to describe the creep behavior of ZCW alloys. The constants given in the first term are for type II alloys and will be slightly smaller for type I alloys.

$T = 1,500$ to $1,800°C$ or 0.48 to 0.56 T_{mp}

$$\dot{\epsilon} = 1.4 \times 10^4 \; \frac{\sigma}{T} \; \exp \; (\frac{-104,000}{RT}); \; \sigma = 5,000 \text{ to } 12,000 \text{ psi} \quad [11]$$

$$\dot{\epsilon} = 2.8 \times 10^{-11} \; \frac{\sigma^{4.6}}{T} \; \exp \; (\frac{-104,000}{RT}); \; \sigma = 14,000 \text{ to } 20,000 \text{ psi} \quad [12]$$

For the constants given, the units of stress are psi, temperature °K.

IV. MODELS FOR CREEP

The dislocation climb model developed by Ansell and Weertman [6] for the creep of dispersion strengthened metals will be compared with the experimental results of the present work. The Nabarro-Herring model for viscous creep will also be compared. These models have been developed in greater detail than other models. The model of Mott [49], mentioned in the Introduction and containing a large stress dependency in the activation energy, cannot possibly satisfy the present experimental results which gave a constant activation energy over the entire stress range studied.

The Ansell-Weertman Model

The Ansell-Weertman model for creep in a dispersion-strengthened material is based on the ideas of Mott [49]. The equations were first developed in detail by Weertman [80,81] for dislocation climb between slip planes in a single phase material. The model [6] was later adapted to the Orowan bowing model for a dispersion strengthened material. The model is given here in considerable detail. It will be shown that the model satisfies the present experimental results on ZOW alloys better than the only other test of the model which was that of Ansell and Lenel [5] on SAP alloys.

Dislocation loops are considered to be created at sources under the action of an applied stress. The loops expand to some maximum radius at which point they are annihilated by climbing to dislocations of opposite sign on neighboring slip planes. For a dispersion-hardened alloy it is reasonable to assume, as suggested by Schoeck [64], that the rate controlling process for steady state creep is the climb of dislocations over the second-phase particles.

A second assumption concerns the origin of the dislocations in a dispersion-strengthened matrix. In a single-phase metal it is usually assumed that there is a three-dimensional network present which provides Frank-Read dislocation sources. In a dispersion-strengthened matrix the usual dislocation network may not be present. Instead, short dislocation line segments may start at one particle and terminate at a neighboring particle. At high stresses these short segments could act

as sources. In developing the equations, Ansell and Weertman first con-
sidered the case where dislocations originate as Frank-Read sources whose
lengths are much greater than the distance between particles. The case
where dislocation segments act as sources occurs at very high stresses
and is not applicable to the present work. This case is described brief-
ly at the end of this section.

Theory at Low Stresses

Several of the parameters are illustrated in Figure 19. Figure 19
(a) pictures a Frank-Read (F-R) source imbedded in a field of the second-
phase particles. The plane of the paper is the slip plane. Figure 19 (b)
shows a cross-sectional view of dislocation loops some time after appli-
cation of a stress. The slip plane is horizontal and perpendicular to
the plane of the paper. Figure 19 (c) shows a view of a length of dislo-
cation line looking down the direction of motion of the dislocation. The
slip plane is again horizontal and perpendicular to the plane of the paper.
The direction of motion of the dislocation is into the paper.

The creep rate was calculated from the model in the following manner.
The creep rate is equal to the product of the number of F-R sources per
unit volume giving off dislocation loops, the plastic strain produced by
one loop upon expansion to its maximum radius, and the rate of production
of loops at one source. The creep rate $\dot{\varepsilon}$ is, therefore, equal to

$$\dot{\varepsilon} = M \pi L^2 b r \qquad [13]$$

where M is the number of sources per unit volume, L is the maximum radius
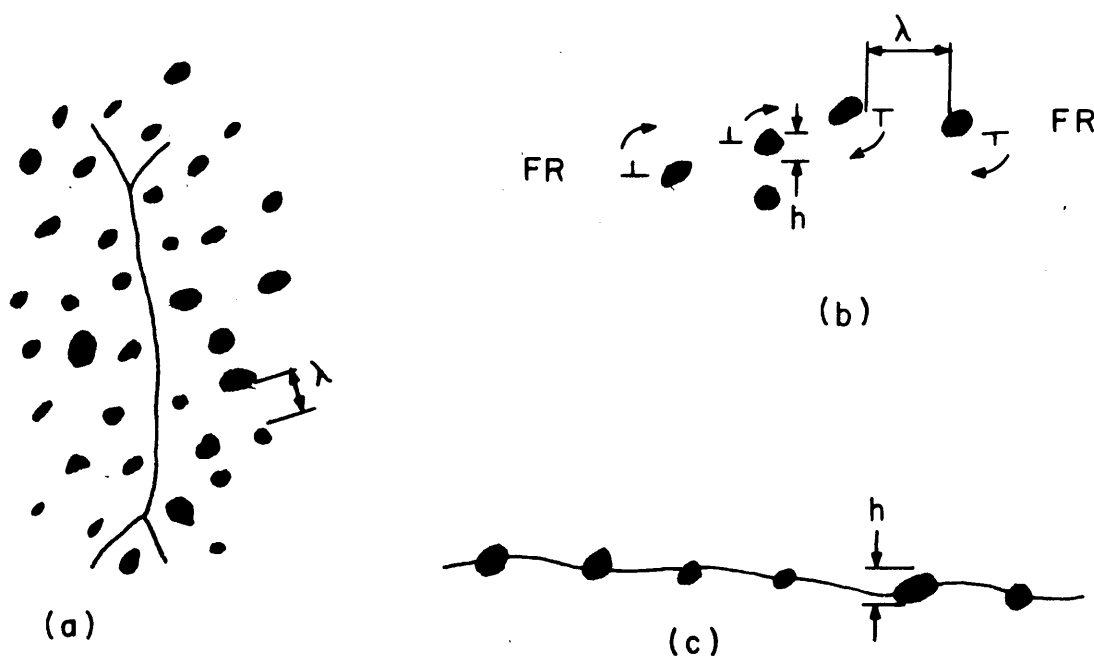
FIGURE 19.-Ansell-Weertman Dispersion Model: (a) Frank-Read source with slip plane in plane of paper; (b) Dislocation loops under stress with slip plane horizontal and perpendicular to plane of paper; arrows indicate direction of climb; (c) Dislocation line as viewed from the direction of motion.

72-49

of the dislocation loop, b is the length of the Burgers vector of a dis-
location, and r is the rate of creation of dislocations at one source.

The maximum radius L was calculated from the following argument.
Consider a pill box of height 2d and radius L, where d is the distance
climbed by a dislocation in order to annihilate a dislocation on a neigh-
boring slip plane. Let one F-R source be situated at the center of the
pill box. The probability that the pill box will contain three other
F-R sources capable of blocking the original F-R source (it takes at
least three other sources to block a dislocation loop,[23/]) is equal to
one third the density of the F-R sources times the volume of the pill
box, or $2\pi ML^2 d/3$. The probability must be essentially one that at the
maximum radius L a dislocation loop is blocked from further expansion
by dislocations on a neighboring slip plane. This condition means that
the value of L must be such that

$$2\pi L^2 d \underset{\sim}{\frac{3}{M}}$$

or $\quad L^2 \underset{\sim}{\frac{1}{2\ Md}}$ [14]

where d is the distance climbed by a dislocation in order to annihilate
a dislocation on a neighboring slip plane. It was assumed that d is of
the order of the dimensions of the particle $(d = h)$.

The rate of creation of dislocations, r, is equal to the rate at
which dislocations surmount the barriers in Figure 19 (b). The rate of
climb over barriers can be calculated in turn from the velocity of climb,
which is controlled by the diffusion of vacancies or interstituals.

Weertman [81/] calculated the velocity of climb for a dislocation which could maintain an equilibrium concentration of vacancies in its vicinity. This velocity is

$$v \sim \frac{\sigma b^2 \, D}{kT} \qquad [15]$$

where σ is the stress, D is the coefficient of self-diffusion, k is Boltzman's constant and T is the absolute temperature. The rate term r is then

$$r = \frac{v}{h} \qquad [16]$$

By combining equations [13], [14], [15], and [16] the creep rate becomes

$$\dot{\varepsilon} = \frac{\pi \sigma \, b^3 \, D}{2kTh^2} \, \frac{1}{2\sqrt{2}} \qquad [17]$$

Where the $2\sqrt{2}$ factor is used to correct for unresolved stress and strain rates.

The range of stress for which equation [17] is valid is based upon the Orowan [56/] criteria for yielding, given by the expression

$$\sigma = \frac{2 \, \mu \, a_0}{\rho} \qquad [18]$$

where σ is the shear stress needed for bending a dislocation line into a curve for radius ρ. The condition for which ρ is equal to the distance between nodes of dislocation network of the F-R sources, L, gives the dislocation generating stress [4/]

$$\sigma = \frac{2 \, \mu \, b}{L} \qquad [19]$$

The condition for which ρ is equal to the interparticle spacing, λ ,
gives the stress at which the dislocations will bypass the particles.

$$\sigma = \frac{2 \mu b}{\lambda} \qquad [20]$$

By combining equations [19] and [20] the limits for the low stress region of the Ansell-Weertman model are

$$\frac{2 \mu b}{L} < \sigma < \frac{2 \mu b}{\lambda} \qquad [21]$$

The denominator terms of equation [21] satisfy the condition that the
radius of the dislocation loop is large compared to the interparticle
spacing; that is, $\frac{1}{L} < \frac{1}{\lambda}$ means $L > \lambda$.

The shear modulus, μ, is defined in the usual way [6]/

$$\mu = \sqrt{\frac{1}{2} \; C_{44} \; (C_{11}-C_{12})} \qquad [22]$$

with C_{ij} being the usual elastic constants, L is the length of an F-R
source, and λ is the interparticle spacing.

Theory at High Stresses

In this case, the stresses are great enough to force dislocations
past particles by pinching off loops around the particles. (The case is
also valid when sources may be dislocation segments between particles).
This process is illustrated in Figure 20 (a). The rate controlling
process now is the climb of pinched-off loops around the particles as
shown in Figure 20 (b). The rate at which pinched off loops are anni-
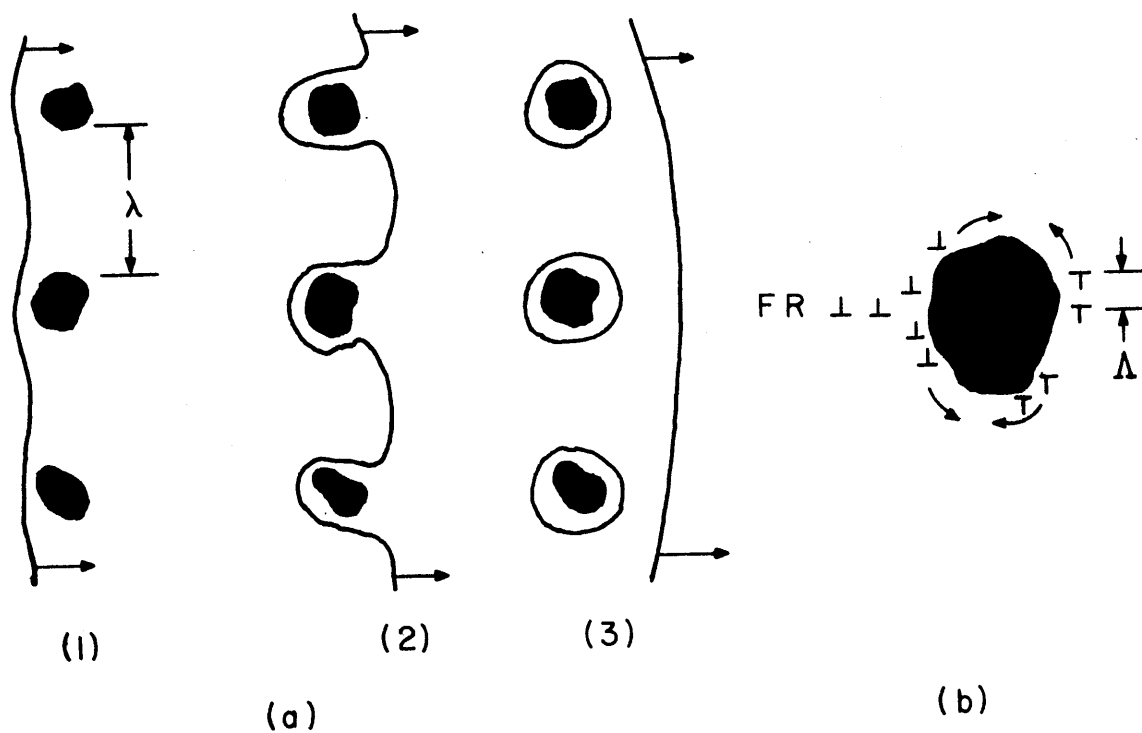
FIGURE 20.-Creep Process at High Stress: (a) Formation of dislocation loops; (b) Climb of dislocations around a particle.

72-77

hilated in Figure 20(b) was estimated. The loops are forced to climb around the particles because of the interaction forces between the loops produced by the interaction forces of the dislocations piled up against the particles. The number N is piled up in the distance λ is

$$N = \frac{2 \, \sigma \, \lambda}{b \, \mu} \qquad [23]$$

The distance a pinched-off loop must climb, Λ, before another loop can be pinched off is of the order $\frac{\mu b}{N \sigma}$; and upon substitution for N

$$\Lambda \sim \frac{\mu^2 b^2}{2 \sigma^2 \, \lambda} \qquad [24]$$

The velocity of climb of the dislocation loop is given by equation [15] with the stress replaced by concentrated stress N and substituting for N from equation [23]

$$v = \frac{2 \, \sigma^2 \, b \, \lambda \, D}{\mu \, KT} \qquad [25]$$

By combining equations [24] and [25] Ansell and Weertman got for the rate r of equation [16] the expression

$$r = \frac{v}{\Lambda} = \frac{4 \, \sigma^4 \, \lambda^2 \, D}{b \mu^3 \, kT} \qquad [26]$$

By combining equations [13], [14], and [26], the creep rate becomes:

$$\dot{\varepsilon} = \frac{2 \, \pi \, \sigma^4 \, \lambda^2 \, D}{h \, \mu^3 \, kT} \, \frac{1}{16 \sqrt{2}} \qquad [27]$$

which is valid for $\sigma > \dfrac{2 \mu b}{\lambda}$ and $n\sigma b^3 < kT$. The factor of $16\sqrt{2}$ exists for correcting unresolved stresses and strains.

At very high stresses where $N\sigma b^3 > kT$ the velocity is no longer given by equation [25]. Ansell and Weertman then gave a $\sigma^2 \exp \sigma^2$ relationship in the very high stress region provided that the included particles are strong enough to withstand the stresses exerted by the dislocations piled up against them. This region of very high stresses was not encountered in subsequent experiments of Ansell and Lenel nor in the present work.

Previous Tests of Creep Model

The first test of the Ansell-Weertman creep model was by Ansell and Weertman [6/] with a SAP alloy designated as MD-2100. The alloy consisted of a very fine dispersion of aluminum oxide plates in a matrix of aluminum. The flakes were 0.013 μm thick by 0.3 μm on edge. The spacing ranged from 0.05 to 1.5 μm with an average spacing of 0.5 μm. The matrix grain size was very small, about 0.5 μm. Thus the grain size was about the same as the particle spacing. The results were unexpected because no steady-state creep was observed and the tests were not reproducible.

The second attempt to test the Ansell-Weertman model was also on a SAP alloy designated as MD-2100 in experiments by Ansell and Lenel. The alloy had a grain size of several millimeters. The particle spacing of 0.9μ was somewhat coarser than the earlier work. The authors were able to show an approximate σ^4 relationship to $\dot{\varepsilon}$ at stresses above $\dfrac{2\mu b}{\lambda}$

in accordance with the theory. In the low stress region, however, the creep rate dropped off sharply and was not in agreement with the linear relationships given by the theory. Again, in the high stress region, the absolute value of creep rate when calculated from equation [27] was about four orders of magnitude greater than their experimental results. They concluded that the density of active dislocation sources in the SAP alloy was abnormally low as compared with the density of active dislocation sources in a single phase metal which is the density used in the model.

No other tests of the Ansell-Weertman model are known.

Nabarro-Herring Model

The Nabarro-Herring model for creep has been well accepted for explaining the creep of single phase alloys at high temperatures [34,46,53]. The model explains viscous flow or linear stress dependency or strain rate by means of vacancy migration. The dimensions of the grains must be approximately 0.1 mm or less.

The energy required to form a vacancy on a grain boundary which is parallel to the stress is different from the energy to form a vacancy on a surface normal to the stress. The energy difference is of the order $\sigma \Omega$ where Ω is the volume of a vacancy. If the stress, σ, is small compared to kT/Ω, the gradient of the vacancy concentration which exists between the surfaces of the grain is approximately equal to

$$2 \frac{C_o}{\ell} \cdot \frac{\sigma \Omega}{kT}$$
[28]

where ℓ is the dimension of the grain and C_0 is the equilibrium vacancy concentration when the applied stress is zero. This gradient in the vacancy concentration gives rise to a vacancy flow by diffusion which introduces the term $D\ell^2$. Upon combining terms the vacancy flow rate is

$$q = \frac{2\ell \, C_0 \, \sigma \, \Omega \, D}{k \, T} \tag{[29]}$$

From the flow rate of vacancies, the rate of change of grain dimensions in the direction of the applied stress was calculated as

$$\dot{\varepsilon} = \frac{B \, \sigma \, \Omega \, D}{\ell^2 \, k \, T} \tag{[30]}$$

The dimensionless constant, B, was calculated by Nabarro and Herring as $\frac{32}{\pi} \simeq 10$; other authors [46] have used the values of 1 or 2 for B.

Viscous creep obeying equation [30] has been observed in many materials at temperatures near $0.8 \, T_{mp}$ and at low stresses.

<u>Fit of ZOW Alloys to Creep Models</u>

A number of creep models [15,22,36,64,82] were considered for fit by the ZOW alloys. All of these except the Ansell-Weertman model and the Nabarro-Herring model were obviously inappropriate because of incorrect functional relationships or conceptional difficulties, eg. no second phase material.

Diffusion Coefficient

The diffusion coefficient is a dominant term in the creep equations because of its exponential dependence upon the activation energy. It is important to use the best possible value for the diffusion coefficient in order to establish fit to a model.

A survey of the literature was made to determine the diffusion coefficient for self diffusion in tungsten. The results of the survey, including the activation energy and the experimental method, are summarized in Table IX. The best value for the activation energy for self diffusion appears to be about 140 Kcal per mole deg. This is appreciably greater than the activation energy for creep of 104 Kcal per mole deg found in this work. The use of a value of 140 Kcal for the activation energy for creep in the model is incompatible with the experimental results because the slope of the curves of $\ln \dot{\epsilon}T$ vs $\frac{1}{T}$ would be in poor agreement. The use of the value of 104 Kcal for the activation energy for creep is in excellent agreement with the work of Gilbert et al [25] who found a value of 105 Kcal for the activation energy for creep for unalloyed tungsten in the temperature range of about 1200 to 2200°C. The close agreement between the present work and that of Gilbert et al.[25] indicates that the activation energy for creep in tungsten is lower than the activation energy for self-diffusion.

The values for D_O as seen in Table IX range from 0.5 to 6.3×10^7 with the better values probably around 0.75 to 11.5. For the present calculations D_O was taken as 2.7 by assuming ΔS was of order k in the usual expression for D_O. An error in D_O will not affect the creep calculations as dramatically as would an error in the activation energy.

Table IX. Investigations of self-diffusion in tungsten

Investigator	Ref.	Year	D_0 cm^2/sec	Activation energy, Q, Kcal/mole deg	Temperature range °C	Experimental method	Remarks
Pawel and Lundy	57	1969	1.88+0.4	140.3+7.2	1300-2400	Isotope tracer with anodic film sectioning	Grain size of 25 microns
Fedorov, et al	21	1969	0.75	116.4	1800-2200	Isotope tracer, sectioning, residual activity	99.8% pure W
Neuman and Hirschwald	55	1967	-	93.1	1950-2100	Isotope electro-transport	
Andelin, et al	1	1965	42.8+4.8	153.1+0.6	2660-3230	Isotope tracer and sectioning	Single crystal
Larikov	43	1966	25.12	151			
Danneberg	18	1961	0.54	120.5			
Von Liempt	79	1945	11.5	140.0	2200-2800	Fe in W extrapolated to zero Fe	
Vasilev and Chernomorchenko	78	1956	6.3 x 10⁷	135.8	1287-1453	Isotope tracer, residual activity at surface	Large D_0 indicates G.B. diffusion

Ansell-Weertman Model

The experimental results of creep in the ZOW alloys do fit the Ansell-Weertman model more completely than any other known experimental work. The strain rates obtained in the present experiments, as shown earlier in Figure 15, were linear in the lower stress range. This is the first instance known to the author in which a linear dependence of creep rate on stress was obtained on a dispersion hardened alloy at such a low homologous temperature. In the high stress region the experimental stress dependence with an exponent of $n = 4.66$ agrees reasonably well with the theoretical value of $n = 4$. The constant value of the activation energy for creep over a wide range of temperature and stress also agrees with the model because the diffusion coefficient is normally a very gradually changing function of temperature and stress.

As a further test of the Ansell-Weertman model the absolute values of the strain rate were calculated from the equations and compared with the experimental values of strain rate. A temperature of 1618°C was selected because more experimental data were available at this temperature. Any other temperature would be equally valid because of the constancy of the activation energy, Q. In the low stress region the values of the constants in equation [17] are

$$b = \frac{1}{3} \ [111] = \frac{\sqrt{3}}{3} \ a_o = 1.82 \times 10^{-8} cm. \quad \text{For } [111] \text{ of tungsten.}$$

$$D = D_o \ exp \ \frac{-Q}{RT} = 2.7 \ exp \ (\frac{-104,000}{1.987 \times 1891}) = 2.3 \times 10^{-12} \ \frac{cm^2}{sec}$$

$k = 1.38 \times 10^{-16}$ erg/°K

$T = 1891°K$

$h = 2 \times 10^{-5}$ cm. Mean particle size of ZrO_2 dispersoid.

Substitution of the above values into equation [21] gives values of creep rate exactly three orders of magnitude greater than the experimental values of creep rate. For example, at a stress of $\sigma = 10,000$ psi $= 6.9 \times 10^8$ dyne per cm^2, the calculated value of strain rate is 5.5×10^{-5} per sec; the experimental value is 5.6×10^{-8} per sec. The same discrepancy of 10^3 between calculated and experimental values of creep rate exists over the temperature range of 1500° to 1800°C and over the stress range of 5,000 to 12,000 psi because of the constant value of the activation energy Q.

The strain rates in the high stress region calculated from equation [27] were compared with the experimental values of strain rate. In addition to the values for the constants already given

$\lambda = 2 \times 10^{-4}$ cm. Mean spacing of ZrO_2 dispersoid

$\mu = 3.73 \times 10^{12} \dfrac{dyne}{cm^2} \times 0.8$. Shear modulus for tungsten.

The factor 0.8 on the shear modulus is to correct for the effect of elevated temperature in accordance with studies on elastic constants made by Armstrong and Brown [7]. Again using a temperature of 1618°C, an activation energy of 104 Kcal per mole deg, but a stress of 16,000 psi $= 1.1 \times 10^9$ dynes per cm^2, the calculated values of strain rate were three orders of magnitude higher than the experimental values. For example,

the calculated strain rate was 2.9×10^{-4} per sec, whereas the experimental value was 2.5×10^{-7} per sec. As before, because of the constancy of the activation energy, the discrepancy of 10^3 will hold over the entire temperature range from 1500 to 1800°C. The difference between calculated and experimental strain rates will vary somewhat with stress because of the difference between the exponent $n = 4$ and $n = 4.66$. This difference is relatively small over the stress range of 14,000 to 20,000 psi.

The discrepancy of 10^3 between the calculated and experimental values of creep rate is similar to the 10^4 discrepancy found by Ansell and Lenel [5] in SAP alloys. The functional dependency of temperature and stress in the high stress region did satisfy the Ansell-Weertman model.

An additional test of the Ansell-Weertman model can be made on the particle spacing for which dislocation by-pass begins. The condition is given by equation [20], $\sigma = \dfrac{2 \mu b}{\lambda}$,

where the stress σ changes from linear to σ^4 dependency. Experimentally, from Figures 16 and 18, the change in stress dependency occurs between 12,000 and 14,000 psi. By setting $\sigma = 13,000$ psi in equation [20] the interparticle spacing λ is found to be 1.2 microns. This is in reasonable agreement with the distance of 2 microns estimated from the microstructure.

Nabarro-Herring Model

The experimental results of creep in the ZOW alloys fit the functional relationships of temperature and stress in the Nabarro-Herring equation

as shown by comparison of equations [11] and [30]. The stress dependency is linear and the temperature dependency is $\frac{1}{T}$ exp $(\frac{-Q}{RT})$ in both cases. An additional check on the validity of the Nabarro-Herring model was made by comparing the calculated and experimental values of strain rate. The mean grain dimension is taken as the mean intercept length $\Delta\ell$. Although $\Delta\ell$ increased slightly during long time creep tests, the value of 8 μm is reasonable. The volume of a vacancy is taken as $\frac{1}{2}$ the volume of a tungsten atom or $\frac{b^3}{2} = 3 \times 10^{-24}$ cm^3. The value of B is taken as 2. The diffusion coefficient is the same as previously mentioned. At a temperature of 1618°C and stress of 10,000 psi = 6.9 x 10^8 dyne per cm^2, the calculated value of strain rate is 6.2 x 10^{-8} per sec. This compares very well with the experimental value of 5.6 x 10^{-8} per sec obtained at this temperature and stress. Thus, in the low stress region the ZOW alloys fit the Nabarro-Herring model with respect to the functional dependence of stress and temperature as well as in the absolute value of strain rate.

Proposed Creep Model for Dispersion Strengthened Alloys

Low Stresses

In the preceding discussion it was shown that both the Ansell-Weertman model and the Nabarro-Herring model give the correct functional dependency of stress and temperature upon creep rate of the ZOW alloys. The Ansell-Weertman model gives creep rate values 10^3 times too large whereas the Nabarro-Herring model gives values of the correct order.

Therefore it appears that the Nabarro-Herring model should be accepted even though it is not normally found to apply at such low homologous temperatures.

Burton and Greenwood [13] have pointed out that the range of linear creep may be extended by high elastic modulus, low stacking fault energy and dispersion in a metal alloy. This lends support to the Nabarro-Herring model for ZOW alloys.

The results of Ansell and Lenel [5] on the SAP alloy also supports the Nabarro-Herring model rather than the Ansell-Weertman model. For the SAP alloy the creep rate fell to very low values in the low stress region where $\sigma < \frac{2 \mu b}{\lambda}$. Ansell and Lenel stated that "At these stresses, the applied stress is probably too low to nucleate dislocations from the sources present in the alloy". The present author feels that this statement may be true and that it also negates the validity of the Ansell-Weertman model in the low stress region. Consideration of the large grain size of several millimeters in the SAP alloy of Ansell and Lenel could easily explain the extremely low creep rate. Using a grain size of 2 mm the creep rate was calculated by the Nabarro-Herring equation [30] for the SAP alloy. At a temperature of 873°K, a stress of 10^8 dyne per cm^2, and other data given by Ansell and Lenel the calculated strain rate of 4×10^{-10} per sec agrees remarkably well with their corresponding experimental value of 3×10^{-10} per sec.

It appears that the correct model for a dispersion strengthened alloy for stresses less than $\frac{2 \mu b}{\lambda}$ and temperatures above $0.5 \, T_{mp}$ is one in which Frank-Read sources are inactive or do not exist because of the dis-

location blocking by the dispersoid phase. Steady state creep occurs
by the diffusion of vacancies and atoms according to the Nabarro-Herring
model.

High Stresses

In a preceding discussion it was shown that the Ansell-Weertman
model gives the correct functional dependency of stress and temperature
upon the creep rate of both ZOW and SAP alloys; however, the values of
creep rate are 10^3 to 10^4 times too high. It is believed that the problem
with the Ansell-Weertman model arises with the volume swept out by a dis-
location which is associated with one unit of climb, b. The assumption
which led to equation [14] allowed a dislocation loop to expand and then
climb through a volume which was three times the volume associated with
the density of sources. Substitution of equation [14] into the basic
creep expression, equation [13], then eliminated the density of sources
M and the loop radius L. The present author believes that the volume
through which a dislocation loop expands and climbs and the volume
associated with three F-R sources are not equivalent in an alloy con-
taining a dispersoid. In the high stress region, when a moving dislocation
passes a particle, the loop which forms around the particle begins to
climb and immediately annihilates the oldest loop near the extreme end
of the particle. Consequently, the area swept out by a dislocation be-
tween successive encounters and by-passing of particles is determined
by the planar interparticle spacing rather than the total area swept out
by the dislocation between three F-R sources.

Consider the area swept out by a dislocation between successive encounter with a particle. Ashby and Ebeling [8] state that the average distance from a particle to its nearest two or three neighbors, as in calculating the interaction between a dislocation and a random array of objects in its slip plane, is at least as large as the interparticle spacing, λ . Ashby and Eberling gave the spacing as 1.18 λ. The area associated with expansion of a dislocation between particle encounters is then on the average equal to $(1.18\lambda)^2$. This term then replaces πL^2 in equation [13] which is used to derive equation [27].

The value for the density of active F-R sources M is less certain. Ansell and Lenel [4] gave a value of 10^9 per cm^3 which appears reasonable for most metals. Substitution of the above values for πL^2 and M in equation [13] and substitution of the other Ansell-Weertman relations as derived before results in the modified equation for the creep rate in the high stress region

$$\dot{\epsilon} = \frac{1.4 \times 10^9 \ \lambda^4 \ \sigma^4 \ D}{\mu^3 \ k \ T} \quad \frac{1}{16} \ \frac{1}{\sqrt{2}} \qquad [31]$$

where the constant has the units of cm^{-3} and $\frac{1}{16} \ \frac{1}{\sqrt{2}}$ corrects for non-resolved stress as before.

The functional dependency of the temperature and the stress in equation [31] remain the same as before and therefore satisfy the experimental results on dispersion strengthened alloys of ZOW and SAP. The values of strain rate calculated by equation [31] agree exceptionally well with the experimental values. For example, for ZOW alloy II   at

1618°C, 16,000 psi stress, and using the values of the other terms as given in the preceeding section, the calculated strain rate is 0.5×10^{-7} per sec; the experimental value of strain rate was 2.5×10^{-7} per sec.

The SAP alloy of Ansel and Lenel [5/] can be easily used to test the modified creep rate equation [31]. Comparison of the Ansell-Weertman equation [27] and the author's equation [31] reveals that the difference between the equation is given by the factor

$$1.4 \times 10^9 \; \lambda^2 \; \times \frac{h}{4\pi} \qquad\qquad [32]$$

The particle spacing of the SAP alloy was given as 0.9×10^{-4} cm and the particle size as 3×10^{-5} cm. Substituting these values into equation [32] gives 0.25×10^{-4}. This factor is of the order needed to account for the discrepancy between the results of Ansell and Lenel and the Ansell-Weertman model.

The absence in equation [31] of the term h, the particle size, is a significant departure from the original equation [27] of Ansell and Weertman. However, this is reasonable for the author's model considering that neither the expression for the distance between dislocation loops climbing a particle, equation [24], nor the expression for the velocity of climb, equation [25], contains a term for the dimension of the particle. Thus it appears that the size of the dispersed particle per se is unimportant but the particle spacing is very significant. From a practical viewpoint the size of the particles is important because a reasonably small volume percentage of dispersed phase cannot provide a small inter-

particle spacing without requiring the dispersed particle to be very small. The smallest size of particle is limited to that which will block dislocations. This dimension would be of order Λ. For smaller particles the behavior of the material would approach that of a solid solution alloy.

An additional comment should be made concerning the discrepancy in the exponent of the stress; $n = 4$ by the theory and $n = 4.66$ by experiment. The Nabarro-Herring creep does not cease to operate in the high stress region but rather is small compared to the creep produced by the climb of the dislocation loops. The contribution of Nabarro-Herring creep could cause the exponent n to be greater than 4.

CONCLUSIONS

From the results of the experiments described on the ZOW alloys, the following are concluded:

1. The structure of the alloys in the as-extruded condition can be converted to a structure with a stable grain size and dispersoid phase of ZrO_2 by heating for 20 hours at 1800°C under vacuum.

2. The microstructure of the stabilized structure was essentially the same for type I, W-0.4Zr-0.05 O as for type II, W-0.7Zr-0.12 O alloy. The grain size was about 7 micron; the ZrO_2 particle size about 0.2 micron; and the planar interparticle spacing about 2 microns.

3. The tensile strength over the temperature range of 1500° to 2000°C compares with the best of any other tungsten alloy in the annealed condition.

4. The stress-rupture lives, interpolated at 1650°C, compare with the best of any other tungsten alloy. Lives ranged from 1.4 to 190 hr.

5. The activation energy for creep was a constant 104,200 $\pm$ 3,200 cal per mole deg over a temperature range of 1500° to 1800°C and a stress range of 3,500 to 20,000 psi. The activation volume was about 2×10^{-21} cm^3.

6. The relation between creep rate and stress at constant temperature was best given by a linear dependency of the form $\dot{\epsilon} = C\sigma$ at stress from 3,500 to 12,000 psi, and by a power dependency of the form $\dot{\epsilon} = C\sigma^n$ where n = 4.66 at high stresses, from 14,000 to 20,000 psi.

7. The functional dependency of the creep rate on stress satisfies the Ansell-Weertman model at both low and high stresses but the values of the creep rate given by the model are about 10^3 times too large.

8. The functional dependency of the creep rate on stress satisfies the Nabarro-Herring model at low stresses. This model gives the correct order for the value of creep rate on ZOW alloys.

9. The proposed model for creep is as follows: For the low stress region where $\sigma < 2 \frac{\mu b}{\lambda}$ the dislocations are so completely locked in by the dispersed particles that creep occurs by

bulk diffusion of vacancies and atoms (Nabarro-Herring creep) rather than by dislocation climb. In the high stress region, $\sigma > \dfrac{2\mu b}{\lambda}$, where the dislocations break away between the particles, the creep rate is controlled by the climb of the residual dislocation loops around the particles. The density of Frank-Read sources is taken as 10^9 per cm^3. The area swept out by a dislocation in providing a unit of climb is of the order λ^2 instead of πL^2 as proposed by Ansell and Weertman.

10.   The proposed model for creep satisfies the experimental results on ZOW and SAP alloys.

BIBLIOGRAPHY

1. Andelin, R. L., J. D. Knight, and M. Kahn. Diffusion of tungsten and rhenium traces in tungsten. Transactions of the Metallurgical Society of AIME 233:19-23. 1965.

2. Ansell, George S. Mechanical properties of two-phase alloys. Chapter 18 of Physical Metallurgy. North-Holland Publishing Company, Amsterdam. R. W. Cahn, editor. p. 887-924. 1965.

3. Ansell, G. S. The mechanism of dispersion strengthening: A Review. Oxide dispersion strengthening. Metallurgical Society Conference Vol. 47. Bolton Landing Conference, New York, June 27-29, 1966. Edited by George S. Ansell, Thomas D. Cooper, and Fritz V. Lenel. Gordon and Breach, Science Publishers, New York. 1968.

4. Ansell, G. S. and F. V. Lenel. Criteria for yielding of disperson-strengthened alloys. Acta Met. 8:612. 1960.

5. Ansell, G. S. and F. V. Lenel. Creep of a recrystallized aluminum SAP-type alloy. Transactions of The Metallurgical Society of AIME 221:452. June 1961.

6. Ansell, G. S. and J. Weertman. Creep of a dispersion-hardened aluminum alloy. Transactions of The Metallurgical Society of AIME 215:838-843. October 1959.

7. Armstrong, Philip E., and Harry L. Brown. Dynamic Youngs modulus measurements above 1,000°C on some pure polycrystalline metals and commercial graphite. Transactions of The Metallurgical Society of AIME 230:962-966. August 1964.

8. Ashby, M. F. and R. Ebeling. On the determination of the number, size, spacing, and volume fraction of spherical second-phase particles from extraction replicas. Transactions of The Metallurgical Society of AIME, Vol. 235, p. 1396. October 1966.

9. Atkinson, R. H. Physical metallurgy of tungsten and tungsten-base alloys. Westinghouse Electric Corporation, WADD-TR-60-37. May 1960.

10. Barth, V. D. and H. O. McIntire. Tungsten powder metallurgy. National Aeronautics and Space Administration Report NASA SP-5035. 39p. November 1965.

11. Blickensderfer, Robert, Mark I. Copeland, and William L. O'Brien. A new internal oxidation process for strengthening tungsten. Washington U. S. Government Printing Office, 1971. 40 p. (U.S. Bureau of Mines Report of Investigations no. 7521).

12. Brammar, I. S. and D. W. Dawe. Metallography of dispersion hardened alloys and its relation to creep resistance. Air Force Materials Laboratory, Aeronautical Systems Division Report ASD-TDR-63-343. Wright-Patterson Air Force Base, Ohio. 61 p. June 1963.

13. Burton, B. and G. W. Greenwood. The limits of the linear relation between stress and strain rate in the creep of copper and copper-zinc alloys. Acta Metallurgica 18:1237. December 1970.

14. Chaudhuri, A. Stress- and temperature-dependence of creep in a nickel-base high-temperature alloy. Journal of the Institute of Metals 98:114-116. 1970.

15. Coble, R. L. A model for boundary diffusion controlled creep in polycrystalline materials. J. Appl. Phys. 34:1679. June 1963.

16. Cook, Charles R. Evaluation of high strength tungsten base alloys. Air Force Materials Laboratory, Wright-Patterson Air Force Base, Ohio. Technical Report AFML-TR-65-397. 115 p. November 1965.

17. Cottrell, A. H. Creep and ageing effects in solid solutions. In: Creep and fracture of metals at high temperatures. A Symposium. National Physical Laboratory, May 31-June 2, 1954. Her Majesty's Printing Office, London. p. 141-156. 1956.

18. Danneberg, W. Metallwirtschaft and Technik. 10:977. 1931.

19. DMIC report 191. Columbus, Ohio 1963. (Battelle Memorial Institute Defense Metals Information Center). The engineering properties of tungsten and tungsten alloys. 128 p.

20. Dorn, J. E. Creep and recovery. Transactions of the American Society for Metals, p. 255-283. 1957.

21. Fedorov, G. B., F. I. Zhomov, and E. A. Smirnov. Self-diffusion of tungsten and niobium and diffusion of tungsten into niobium. Metalloved. Chist. Metal. no. 8, p. 145-153. 1969.

22. Fisher, J. C., E. W. Hart, and R. H. Pry. The hardening of metal crystals by precipitate particles. Acta Met. 1:336. May 1953.

23. Fridel, J. On the linear work hardening rate of face-centered cubic crystals. Phil Mag. 46:1169. 1955.

24. Garofalo, Frank. Fundamentals of creep and creep-rupture in metals. The Macmillan Company, New York. 1965. 258p.

25. Gilbert, E. R., J. E. Flinn and F. L. Yagee. Multimechanism behavior in the creep of tungsten. The Fourth Symposium on refractory metals. Transactions of the Metallurgical Society of AIME, French Lick, Indiana. 25p. 1965.

26. Green, Walter V. Short-time creep-rupture behavior of tungsten at 2250° to 2800°C. Transactions of AIME 215:1057. 1959.

27. Goodspeed, R. C. and G. W. King. Development of high strength tungsten-thoria alloy sheet. Air Force Materials Laboratory, Wright-Patterson Air Force Base, Ohio. Technical Report AFML-TR-69-22. 63p. 1969.

28. Grant, Nicholas J. and Arthur W. Mullendore. Deformation and fracture at elevated temperatures. Massachusetts Institute of Technology Pres, Cambridge, Mass. 1965. 211p.

29. Grierson, Robert and L. J. Bonis. Basic studies on dispersion hardening. National Aeronautics and Space Administration Report NASA CR-360. 59p. 1966.

30. Guyot, P. Activation energy and activation volume in S.A.P., letter to the editor. Acta Metallurgica 12(5):665-667. 1962.

31. Guyot, P. On the mechanisms of deformation in dispersion hardened alloys. University of California, Lawrence Radiation Laboratory Report UCRL-16803, 31p. 1966.

32. Hansen, Niels. Dispersion-strengthened aluminum products manufactured by powder blending. Powder Metallurgy 12(no. 23):4. 1969.

33. Herbell, Thomas P., John W. Weeton, and Max Quatinez. Structure and properties of tungsten-base powder metallurgy composites. National Aeronautics and Space Administration Technical Note, NASA TN D-3610, September 1966, 48p.

34. Herring, Conyers. Diffusional viscosity of a polycrystalline solid. J. Appl. Phys. 21:437. May 1950.

35. Institute of Metals. Symposium on internal stresses in metals and alloys held in London on 15th and 16th October 1947. The Institute of Metals, 4 Grosvenor Gardens, London, S. W. I. 1948.

36. Ivanov, L. I., E. A. Abramyan, and V. A. Yanushkevich. Priroda Vysokotemperaturnoi Polyzuchesti Tugoplavkskh Metallov I Splavov. (The nature of high-temperature creep in refractory metlas and alloys). Struktura i Svoystva Zharoprychnykh Metallicheskikh Materialov. USSR, 1967. Translated by U. S. Army Foreign Science and Technology Center, FSTC-HT-23-433-70.

37. Jefferies, Z. The Trend in science of metals. Transactions of AIME vol. 70, p. 303. 1924.

38. Kane, J. S. The use of nitrides for dispersion strengthening of refractory metals. Lawrence Radiation Laboratory report UCRL-50487. August 6, 1968. 11p.

39. Kauzman, Walter. Flow of solid metals from the standpoint of the chemical-rate theory. Transactions of the American Institute of Mining and Metallurgical Engineers 143:57-83. 1941.

40. Klopp, W. D. and W. R. Witzke. Mechanical properties of a tungsten 23.4 percent rhenium 0.27 percent hafnium-carbon alloy. Journal of the Less-Common Metals 24:427-443. 1971.

41. King, George W. An investigation of the yield strength of a dispersion-hardened W-3.8 vol pct ThO_2 alloy. Transactions of the AIME 245:83. 1969.

42. Kocks, U. F. On the spacing of dispersed obstacles. Acta Metallurgicia Vol. 14, p. 1629-1631. 1966.

43. Larikov, L. N. Properties and applications of heat resisting alloys. Svoistva i primmenenie zharoprochnykh splvov, Izd. "Nauk", p. 28. 1966.

44. McCoy, H. E. Creep-rupture properties of tungsten and tungsten-base alloys. Oak Ridge National Laboratory report ORNL-3992. 50p. 1966.

45. McCoy, H. E., R. L. Stephenson, and J. R. Weir, Jr. Mechanical properties of some refractory metals and their alloys. Oak Ridge National Laboratory report ORNL-3593. April 1964. 42p.

46. McLean, D. Mechanical properties of metals. John Wiley & Sons, Inc., New York. p. 285-334. 1962.

47. Milicka, K., J. Cadek and P. Rys. Creep of aluminum strengthened by alumina particles. Acta Metallurgica 18:733-746. 1970.

48. Morcom, W. R. and N. F. Cerulli. Stability of selected submicron refractory dispersoids in tungsten. Modern Developments in Powder Metallurgy. V2 Applications. Plenum Press, New York. Henry Hausner, editor. p. 203-205. 1966.

49. Mott, N. F., A discussion of some models of the rate determining process in creep. National Physics Laboratory Symposium on Creep and Fracture of Metals at High Temperatures. Her Majesty's Printing Office, London. p. 21. 1955.

50. Mukherjee,T., W. E. Stumpf, and C. M. Sellars. Quantitative assessment of extraction replicas for particle analysis. Journal of Materials Science 3:127. 1968.

51. Murphy, Richard J. and Nicholas J. Grant. Investigation of the strengthening mechanisms of dispersion strengthened alloys. Research and Technology Division, Wright-Patterson Air Force Base, Ohio, Technical Documentary Report ASD-TDR-62-734, Part II, July 1964, 28p.

52. Murphy, Richard J., Varadachari Sadagopan, and Nicholas J. Grant. Investigation of the strengthening mechanisms of dispersion-strengthened alloys. Aeronautical Systems Division, Wright-Patterson Air Force Base, Ohio, Technical Documentary Report ASD-TDR-62-734, November 1962. 24p.

53. Nabarro, F. R. N. Deformation of crystals by the motion of single ions. Rep. Conf. "Strength of Solids", 1947, Phys. Soc. Lond. 75:90. 1948.

54. National Physical Laboratory. Creep and fracture of metals at high temperatures. London. Her Majesty's Stationery Office. 1956.

55. Neumann, G. M., and W. Hirschwald. Diffusion of W^{185} in wolfram by electrotransport. Z. Naturforsch, A22, no. 3, p. 388-392. 1967.

56. Orowan, E. Internal stresses - Discussion. Symposium on Internal Stresses in Metals and Alloys, held in London on October 15 and 16, 1947. p. 451-452.

57. Pawel, R. E. and T. S. Lundy. Tracer diffusion in tungsten. Acta Metallurgicia 17(8):979-988. 1969.

58. Quatinetz, Max, John W. Weeton, and Thomas Herbell. Studies of tungsten composites containing fibered or reacted additives. National Aeronautics and Space Administration Technical Note, NASA-TN- D-2757, April 1965. 34p.

59. Raffo, Peter L. Dynamic strain ageing during creep of a Mo-Ti-C alloy. Transactions Quarterly of American Society for Metals V62, no. 4, p. 846-851. 1969.

60. Raffo, Peter L. and William D. Klopp. Mechanical properties of solid-solution and carbide-strengthened arc-melted tungsten alloys. National Aeronautics and Space Administration Technical Note NASA TN D-3240. February 1966. 35p.

61. Rezek, J. and B. G. Childs. Structure and properties of yttria-zirconium dispersions. Journal of Nuclear Materials 26:285. 1968.

62. Schmidt, Fritz F. and Edwin S. Bartlett. The mechanical behavior of refractory-metal alloys. Battelle Technical Review, Vol. 16, no. 1. p. 8-14. 1967.

63. Schmidt, F. F. and H. R. Ogden. The engineering properties of tungsten and tungsten alloys. Defense Metals Information Center, Battelle Memorial Institute, DMIC Report 191. September 27, 1963. 128p.

64. Schoeck, Gunther. Creep and recovery. American Society for Metals, Cleveland, Ohio. p. 199-226. 1957.

65. Seigle, L. L. Solid solution strengthening of refractory metals. Agard Conference on Refractory Metals. Oslo-Blindern, Norway, 41p. 1963.

66. Sell, Heinz G., George H. Keith, Ronald C. Koo, Randolph H. Schnitzel, and Richard Corth. Physical metallurgy of tungsten and tungsten-base alloys. Aeronautical Systems Division, Wright-Patterson Air Force Base, Ohio. WADD Technical Report 60-37, Part II. 143p. 1961.

67. Sell, Heinz G., George H. Keith, Randolph H. Schnitzel and N. Francis Cerulli. Physical metallurgy of tungsten and tungsten-base alloys. Air Force Materials Laboratory, Wright-Patterson Air Force Base, Ohio. Technical Report No. WADD-TR-60-37, Part IV. 103p. 1963.

68. Sell, Heinz G., George H. Keith, Randolph H. Schnitzel and N. Francis Cerulli. Physical metallurgy of tungsten and tungsten-base alloys. Air Force Materials Laboratory, Wright-Patterson Air Force Base, Ohio. Technical Report No. WADD-TR-60-37, Part V, 97p. 1964.

69. Sell, Heinz G., William R. Morcom, George W. King, and N. Francis Cerulli. Development of dispersion strengthened tungsten base alloys. Air Force Materials Laboratory, Wright-Patterson Air Force Base, Ohio. Technical Report No. AFML-TR-65-407, Part I, 89p. 1965.

70. Sell, Heinz G., William R. Morcom, George W. King, and N. Francis Cerulli. Development of dispersion strengthened tungsten base alloys. Air Force Materials Laboratory, Wright-Patterson Air Force Base, Ohio. Technical Report No. AFML-TR-65-407, Part II. 112p. 1966.

71. Semchyshem, M. and E. Kahns. Tungsten-base alloy development. In: Refractory Metals and Alloys IV. Research and Development Vol. 1. Proceedings of the Metallurgical Society Conference, French Lick, Indiana. October 3-5, 1965. Gordon and Breach, 1967. p. 469-499.

72. Singhal, L. K. Yield strength of dispersion hardened B.C.C. materials. International Journal of Powder Metallurgy 7(1):58. 1971.

73. Stephens, Joseph R. Effect of oxygen on mechanical properties of tungsten. National Aeronautics and Space Administration Technical Note NASA TN D-1581. 23p. 1963.

74. Stiegler, James O. A study of the formation of creep cavities in powder-metallurgy tunsgsten. Oak Ridge National Laboratory Report ORNL-TM-3350. 200p. 1971.

75. Takahashi, Sennosuke, Keuchi Iida, and Masao Adachi. Creep of dispersion-strengthened Ni-Al$_2$O$_3$ alloys. Transactions of National Research Institute of Metals 6(6):376, Tokyo. 1964.

76. Taylor, J. L., D. H. Boone, and O. W. Simmons. Effect of grain size and impurities on tensile strength and ductility of tungsten from 2500° to 5000°F in vacuum. Jet Propulsion Laboratory, California Institute of Technology, Technical Report no. 32-632. 9p. July 1, 1964.

77. United States Atomic Energy Commission. Fourth Annual Report. High-temperature materials and reactor component development programs. Vol. 1, Materials. GEMP-334A. February 26, 1965. p. 17-50.

78. Vasilev, V. P. and S. G. Chernomorenko. Isotope tracer diffusion in tungsten. Zavodskaia Laboritoriia 22:688. 1956.

79. Von Liempt, J. A. Die diffusion Wolfram mit niedrigen eisengehalt. Recueil Des Travaux Chimiques Des Pays-Bas 64:239. 1945.

80. Weertman, J. Steady-state creep through dislocation climb. Journal of Applied Physics 55(3):362-364. 1957.

81. Weertman, J. Theory of steady-state creep based on dislocation climb. Journal of Applied Physics 26(10):1213-1217. 1955.

82. Weertman, J. Dislocation climb theory of steady-state creep. Transactions of American Society for Metals. Quarterly 61(4):681-694. 1968.

83. Wilcox, R. A. and A. H. Clauer. Creep of dispersion strengthened nickel-chromium alloys. Symposium on Dislocation Climb and High-Temperature Creep Processes, Materials Engineering Congress, American Society for Metals, Detroit, Michigan 15-17 October 1968.

84. Wilcox, R. A. and A. H. Clauer. Steady-state creep of dispersion-strengthened metals. National Aeronautics and Space Administration Report NASA CR-4639. August 19,1966. 36p. plus 4p. Appendix.

APPENDICES

APPENDIX I

STEADY STATE CREEP EXPERIMENTAL DATA

IN CHRONOLOGICAL ORDER

Alloy type	ZOW No.	Run No.	Approx. test time, hrs	α, psi	Temp °C	$\dot{\varepsilon} \times 10^{-7}$ per sec	Remarks
I	17A	1	18	10,000	1577	0.264	Temp. fluctuations
I	17A	2	7	10,000	1679	0.767	Too short time
I	17A	3	16	10,000	1670	0.708	Poor temp. control
I	17A	4	30	10,000	1678	0.583	T.C. failure
I	17A	5	12	10,000	1808	4.87	
I	17A	6	16	10,000	1573	0.450	Into stage III
I	18A	1	16	10,000	1628	0.585	
I	18A	2	27	10,000	1545	0.165	
I	18A	3	10	10,000	1632	0.570	
I	18A	4	10	10,000	1687	1.05	
I	18A	5	7	10,000	1801	5.31	Stage III began at end of test
II	27B	1	44	10,000	1570	0.295	
II	27B	2	8	10,000	1740	2.97	
II	27B	3	17	7,200	1741	1.52	
II	27B	4	22	7,200	1684	0.770	
II	27B	5	23	7,200	1626	0.384	
II	27B	6	6	7,200	1791	3.10	
II	27B	7	15	7,200	1627	0.621	Into stage III
I	18B	1	42	10,000	1578	0.25	Room temp. variation
I	18B	2	7	10,000	1742	2.56	
I	18B	3	13	7,200	1742	1.05	
I	18B	4	46	7,200	1627	0.300	
I	18B	5	12	7,200	1685	0.605	
I	18B	6	17	5,000	1743	0.625	
I	18B	7	7	7,200	1782	2.47	
II	28A	1	22	10,000	1580	0.358	
II	28A	2	4	20,000	1582	3.84	
II	28A	3	5	20,000	1534	1.64	
II	28A	4	12	20,000	1465	0.517	
II	28A	5	5	20,000	1632	10.8	Into stage III

Appendix I continued

Alloy type	ZOW No.	Run No.	Approx. test time, hrs	α, psi	Temp °C	$\dot{\epsilon} \times 10^{-7}$ per sec	Remarks
II	28B	1	18	10,000	1629	0.604	
II	28B	2	44	5,000	1626	0.115	
II	28B	3	8	5,000	1792	1.04	
II	28B	4	18	5,000	1701	0.315	
II	28B	5	6	5,000	1924	7.27	
II	29A	1	42	7,200	1582	0.200	
II	29A	2	5	20,000	1630	6.78	
II	29A	3	16	10,000	1671	1.15	
II	29A	4	6	5,000	1852	3.10	
II	29A	5	2	5,000	1902	6.72	
II	29B	1	40	14,000	1511	0.234	
II	29B	2	8	14,000	1671	2.41	
II	29B	3	93	3,500	1603	0.0562	
II	29B	4	25	3,500	1801	0.709	
II	29B	5	7	3,500	1886	2.30	
I	22A	1	22	7,200	1618	0.226	
I	22A	2	7	5,000	1748	0.757	Temp. rise and power failure
I	22A	3	10	20,000	1484	0.740	
I	22A	4	12	5,000	1744	0.494	
I	22A	5	4	20,000	1620	7.69	
II	35B	1	21	7,200	1618	0.732	
II	35B	2	5	16,000	1618	7.46	
II	36C	1	16	7,200	1618	0.426	
II	36C	2	3	10,000	1618	0.647	
II	36C	3	2	16,000	1618	2.72	
II	36C	4	0.3	20,000	1618	7.37	
II	36C	5	9	10,000	1619	0.612	
II	36C	6	11	5,000	1618	0.110	
II	36C	7	3	14,000	1619	1.42	
II	36C	8	2	20,000	1620	7.95	
II	36C	9	2	12,000	1620	0.870	

DIMENSIONS OF CREEP SPECIMENS
REDUCTION IN AREA AND ELONGATION

ZOW	Diameter, in [1]		Area, in^2		Reduction in area pct	Elongation pct
	Initial	Final	Initial	Final		
17A	0.126	0.124	0.01247	0.01208	3.1	4.6
18A	0.1253	0.1240	0.01233	0.01208	2.0	2.0
27B	0.1252	0.1230	0.01231	0.01188	3.5	4.0
18B	0.1261	0.1245	0.01249	0.01217	2.5	2.6
28A	0.1276	0.1255	0.01279	0.01237	3.3	4.0
28B	0.1232	0.1220	0.01192	0.01169	1.9	3.3 [2]
29A	0.1255	0.1238	0.01237	0.01204	2.6	3.3
29B	0.1242	0.1230	0.01211	0.01188	1.9	1.9
22A	0.1201	0.1190	0.01133	0.01112	1.9	1.3
35B	0.1210	0.1200	0.01150	0.01131	1.7	1.8 [2]
36C	0.1210	0.1200	0.01150	0.01131	1.7	

[1] After all runs on the specimen.

[2] Broken during removal from creep fixture.